Online Battery State of Health Estimation Method using an H-Bridge and Bi-Directional Converter Circuit.

Javier Hoogendijk Abril

19/07/2024

UNIVERSITY OF TWENTE.

Abstract

The growing use of battery-intensive technology has driven the requirement for accurate and efficient methods to determine the State of Health (SoH) of batteries. This paper describes a novel SoH estimation concept, using a Cascaded H-Bridge (CHB) which facilitates battery parameter estimations for different State of Charges (SoC). The concept consists of a Bi-Directional Converter circuit that delivers a Hybrid Power Pulse Characterisation (HPPC) signal to the battery. The CHB provides the converter circuit with a constant DC voltage from an AC power grid input voltage. Current and voltage sensors record the data, and a MATLAB data-fitting script is utilized to obtain the battery parameters.

To verify that this SoH estimation concept works, a representative Equivalent Circuit Model, namely a Dual Polarisation Battery Model (DPM) is created in SimuLink MATLAB. Comparison of the DPM outcome parameters against the initial input parameters, estimated for different SoC settings, reveal relatively minor errors which indicate that this SoH estimation concept has merit. These errors are mainly related to limitations in the modelling set-up like sampling rate, simulation step size, data fitting algorithms. The DPM including a CHB still resulted in an unsatisfactory large error range which could not be resolved on time.

Contents

1 Introduction **4**

2 Analysis **5**
2.1 State of Health Estimation 5
2.2 State of Charge 5
2.3 Equivalent Circuit Model 6
2.3.1 Dual Polarisation Model 7
2.3.2 Parameter Identification 8
2.3.3 State of Charge Derivation 10
2.4 Hybrid Power Pulse Characterisation 10
2.5 Data Fitting Model 11
2.6 Cascaded H-Bridge 11
2.7 Bi-Directional DC-DC Buck Boost Converter Circuit 15

3 Methodology **17**
3.1 Battery 17
3.2 Dual Polarisation Equivalent Circuit Model Parameter Derivation 17
3.3 State of Charge 18
3.4 Hybrid Power Pulse Characterisation Test Set-up 19
3.5 Data Fitting Model Selection 19
3.6 H-Bridge and Bi-Directional Converter Circuit 19

4 Results **22**
4.1 Initial Dual Polarisation Model Results 22
4.1.1 Estimated Parameter Values 22
4.1.2 Voltage Response 23
4.2 Complete Dual Polarisation Model Results 24
4.2.1 Estimated Parameter Values 24
4.2.2 Voltage Response 26
4.2.3 State of Charge 27
4.2.4 Current Graphs from Bi-Directional Converter 28
4.2.5 DC Voltage Graph of H-Bridge 29
4.3 ECM Parameter Value Comparison 30

5 Discussion **33**
5.1 Initial Dual Polarisation Model Discussion 33
5.2 Complete Circuit Model Discussion 33
5.3 Comparison Between Initial and Complete Circuit Models 34

6 Conclusion **35**

7 Appendix **36**
7.1 AI Statement 36
7.2 Initial Estimated Parameter Values 36
7.3 Voltage Response of Initial Dual Polarisation Model 36
7.4 Complete Circuit Estimated Parameter Values 40
7.4.1 Voltage Response of Complete Dual Polarisation Model 40

References **43**

1 Introduction

In modern-day technology, battery usage is rapidly becoming more prominent. As an example, in the rapid development of electric cars and other battery-intensive technologies, large arrays of batteries are needed to provide power to enable these systems to work. Although this fast development pace of the technology is good, there are still many issues to be solved around the fully electric technology. One important issue with this technology is that the performance and efficiency of a battery decrease the more times or the longer the battery is used and charged [1]. Therefore, each battery has a performance lifespan determined by a threshold limit at which batteries are deemed unreliable and by which they need to be replaced [1]. Another problem or issue is that all battery cells are different, even when they are produced by the same manufacturer. The efficiency of each battery is based on its microscopic composition, which is difficult to fully control during the manufacturing phase [1]. Furthermore, the efficiency of an entire array of batteries is dependent on the least efficient battery [2]. Due to this, it is essential to know which battery is causing issues, so that it can be replaced. To do this, the State of Health (SoH) of the batteries needs to be determined. For this it is critical to determine the remaining charge in the battery, the State of Charge (SoC), which is essential in predicting the battery's performance, efficiency, and lifespan [3]. Measuring battery SoC is not a straightforward process. Several methods, subdivided in 'online' or 'offline' methods, each with its advantages and disadvantages, can be used to determine the State of Charge (SoC) of batteries [4,5]. The advantage of online methods is that the battery is not disconnected from its circuit during battery health testing as is the case for offline methods [4, 5]. Drawback is that this limits the kind of tests that can be performed during online testing [4, 5]. Offline or 'direct' methods involve measuring the battery's actual electrical charge [4,5]. Therefore, these methods are the most accurate, but as they require specialised equipment, these methods can be difficult to implement and can be time-consuming [4, 5]. Online or 'indirect' methods estimate the SoC based on the battery's voltage, temperature, and other characteristics [4, 5]. These methods are less accurate than offline methods but are easier to implement and thereby less expensive [4].

The goal of this thesis is to develop an online State of Health (SoH) estimation method and to simulate a working prototype of a complete SoH estimation method using a Cascaded H-Bridge (CHB) with a Bi-Directional DC-DC converter for varying State of Charges (SoC) of a battery. This will be done via Simulink, a MATLAB simulation program [6].

The outline of the paper is as follows: Section 2 ('Analysis') summarises definitions and background information regarding State of Health (SoH), State of Charge (SoC), Equivalent Circuit Models (ECM), Hybrid Power Pulse Characterization (HPPC), Data Fitting Models (DFM), Cascaded H-Bridge (CHB), and Bi-Directional converter. Section 3 ('Methodology') describes the methodology of the MATLAB simulations and the set-up for the battery SoH testing. The simulation testing results are described in Section 4 ('Results') and the simulation outcomes are presented and discussed in Section 5 ('Discussion'). Finally, the conclusions of this thesis are presented in Section 6.

2 Analysis

To understand the objective of this thesis paper, some background information and definitions are required regarding the different aspects of the project, which are summarised in the following sub-sections. The 'State of Health Estimation' (SoH) sub-section presents its definition and outlines some factors that have a deteriorating effect on the battery's health. In the sub-section 'State of Charge' (SoC) the estimation methodology that defines the battery's health is presented. The 'Equivalent Circuit Models' (ECM) sub-section delves into the particulars of the battery model chosen for the MATLAB simulations in this paper. The subsequent sub-sections 'Hybrid Power Pulse Characterisation' (HPPC), 'Data Fitting Models' (DFM), 'Cascaded H-Bridge' (CHB), and Bi-Directional converter circuit delve more specifically, on how the battery model parameters are determined and how the testing set-up is achieved for the battery model parameter estimation.

2.1 State of Health Estimation

The State of Health (SoH) of a battery can be defined as the ratio of the current maximum capacity relative to the battery's maximum nominal capacity [7]. In other words, the State of Health of the battery is the ratio of the battery's maximum capacity at its current state of usage in relation to the battery's maximum capacity as stated in the battery specifications from the manufacturers. This can also be described as the equation below.

$$SoH(t) = \frac{Q_{max}(t)}{Q_n} \cdot 100\% \tag{1}$$

Where Q_{max} is the current maximum battery capacity, and Q_n is the nominal capacity of the battery as stated in the battery specifications from the manufacturers [7].
The more used the battery is, the less 'health' it has as batteries begin to deteriorate with time due to various factors [1,4]. One factor is related to the chemical reactions that occur within the battery, and which decreases in efficiency the longer the battery is used. This is also often referred to as 'battery aging' [1, 4]. Other factors include the temperature of the battery, the internal resistance of the battery, and the charge-discharge rate (also referred to as cycling rate) of the battery, which also negatively impact the 'health' of the battery if not used under correct conditions [1, 4]. High temperatures accelerate the chemical reactions, and vice versa, lower temperatures decrease the chemical corrections [8]. Extreme temperatures can damage the battery and reduce its lifespan [8]. Hence, batteries must be operated within a specific temperature range according to the battery specifications [8]. Cycling rate refers to the process of charging and discharging a battery [9]. The charge-discharge rate refers not only to how the battery sends power, but also how it is able to charge after it has been depleted in cases of rechargeable batteries [4]. Each charge-discharge cycle affects the battery health due to the accumulation of irreversible chemical reactions within the battery [9]. This is closely linked to the internal resistance of the battery. As the battery has been used for a longer time, it has been observed that the internal resistance of the battery increases, which affects the charge-discharge rate of the battery [9, 10]. All these factors contribute to the health of the battery, and should be considered when estimating the remaining health of a battery.

2.2 State of Charge

Whereas the State of Health (SoH) indicates the overall health of the battery and how much it has degraded over time, the State of Charge (SoC) of the battery is the terminology used to define the amount of charge of the battery at its present state, i.e., it is a measure of how much charge is left in the battery relative to its initial maximum capacity (Nominal Capacity, Q_n). This can described as the equation below.

$$SoC(t) = \frac{Q(t)}{Q_n} \cdot 100\% \tag{2}$$

Similar to the state of health, the total SoC of a battery can change due to many factors such as temperature, internal resistance, battery use, etc., which all negatively affect the battery's

effectiveness during the battery's life-cycle. As the State of Charge (SoC) capacity of the battery is progressively decreasing during its lifespan, many battery manufacturers set a minimum limit for maximum SoC capacity below which batteries are deemed unreliable and unusable. In most cases, especially in electrical vehicles and everyday electronic devices, this minimum capacity limit for maximum SoC is set at 80% of its Nominal Capacity [1]. This hard limit is set for many reasons such as to secure adequate battery performance and reliability by limiting the allowable decrease of power that the batteries in use can deliver, to secure a sufficient charge and discharge rate of the batteries, to prevent that the batteries reach temperatures exceeding the specified temperature range when being used, which all can occur as battery health deteriorates [1]. All these factors affect the performance of the battery system and can cause issues when batteries over-used [1].
From Equation 2 and Equation 1 it can be concluded that the State of Health (SoH) of a battery is determined by the maximum achievable charge capacity, i.e., the maximum State of Charge (SoC) of that battery at that moment in time. As previously mentioned, the maximum charge capacity of a battery slowly decreases during its lifespan due to various factors. By measuring the maximum SoC capacity of the battery at any given time, and dividing it by its rated nominal capacity, the State of Health of the battery can be determined.

2.3 Equivalent Circuit Model

To be able to calculate the State of Charge (SoC) of a battery, a model of the battery along with its parameters needs to be determined for different initial voltages. This can be done through the use of an Equivalent Circuit Model (ECM) [11–13]. An ECM is a simplistic representation of the battery, and the different internal components that form the battery [11–13].
The accuracy of the ECM is determined by a combination of three different factors, namely (1) the number of battery elements/characteristics that are required to be modelled which determines the complexity of the ECM, (2) the accuracy of the method(s) that is(are) applied to measure the battery parameters that need to be modelled, and (3) the type and accuracy of test profile that is used to measure the battery parameters [11].
Regarding the first factor, a simpler model results in less accurate parameters as the model design of the ECM limits the number of internal battery elements accounted for [11]. This can be seen in ECMs such as the Rint Model (Figure 1a), which consists of only a voltage source as the Open Circuit Voltage (OCV) and a resistor, which can model a limited amount of the characteristics of a battery [11, 13, 14]. A slightly more complex model, the Thevenin Model, consists of the same building blocks as the Rint Model but with an additional parallel resistor and capacitor (RC) pair [11]. This allows it to model additional battery characteristics compared to the Rint Model. An even more complex ECM, such as the Dual Polarisation (DP) Model (Figure 1b), consists of a voltage source similar to the Rint model, but then includes two parallel RC pairs in series, which thereby allows for even more of the characteristics of the battery to be modeled [11–15]. Understandably, increasing the complexity of the ECM allows for more battery characteristics to be modeled, while a simple model can only portray a few of the battery characteristics. Although it might appear counter-intuitive, in some cases it actually might be beneficial simplifying the ECM, i.e., concentrating on modelling a few key elements instead of all possible elements of the battery, allowing for a better understanding of the battery that is being investigated [13]. This would also allow to use less complex equations to describe the battery characteristics [12, 15]. Another benefit of the ECM design is the flexibility of the model [12]. As alluded to previously, the complexity of the battery model can be adjusted by the number of RC pairs included in the ECM to achieve the desired accuracy [12]. The drawback of adding more RC pairs, as stated in [13, 14], is that the computational complexity increases while the level of accuracy doesn't significantly change. Therefore, there is an efficiency limit between the amount of RC pairs added to the ECM model and the added accuracy of the model

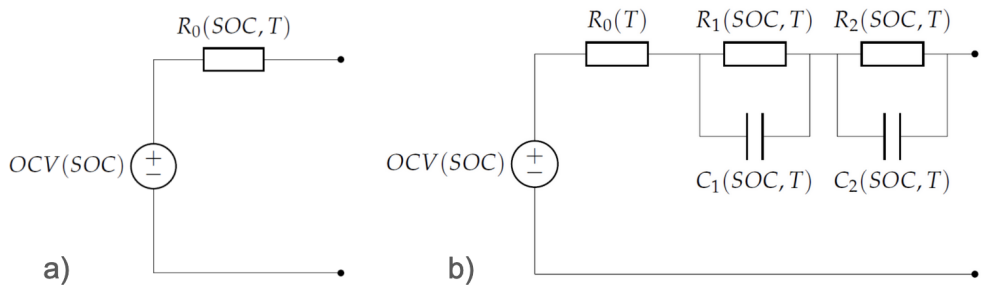

Figure 1: Example of (a) Rint Model and (b) Dual-Polarisation Battery Model [14]

The second factor that impacts the accuracy of the ECM is the method by which the battery parameters are obtained [11]. Some more complex and direct methods, such as Electrical Impedance Spectrometry (EIS), can achieve a higher level of accuracy for parameter identification compared to simpler methods [4]. EIS is an experimental direct measurement method that is used to study the electrochemical process inside the battery [4]. Although this might be beneficial, complex battery parameter measurement methods might not be advantageous due to the resulting increase in computational complexity, as well as the need for complex models to visualize the system in question [14]. The EIS is an offline method as the battery needs to be removed from its initial circuit for its parameters to be tested and identified through a long experimental process [4]. As stated in [5], EIS is considered an effective methodology for SoH estimations, especially since the estimations could be further improved by integrating it with other measurement methods to derive a more comprehensive and effective battery model, although it currently has an error rate of 3.73%. An alternative, online measurement method that could be considered is using Hybrid Power Pulse Characterisation (HPPC) (see subsection 2.4). This particular method consists of sending the battery short positive and negative current pulses [16]. One important factor of HPPC is being able to measure the current pulses and the voltage response of the battery, therefore an additional circuit may need to be added to be able to conduct measurements during HPPC testing. From the voltage response of the circuit, the parameters of the battery can be estimated using machine learning software, linear-regression approximation estimations, and data-fitting models [17]. Each of these combined HPPC and data-fitting model methods has its own accuracy due to the different constraints and complexity in which each method works. Therefore, similar to the ECM, there is a limit and/or trade-off between which methods provide the best measurement accuracy and what level of computational complexity is required for modeling those measurement methods.
The third factor that impacts the accuracy of the ECM is related to the test profile that is carried out to measure the battery parameters [11]. Test profiles can vary depending on the information that is wanted from the experiment. Some test profiles such as the Cycle Experiment, Open-Circuit Voltage Experiment, and Hybrid Power Pulse Characterisation (HPPC) test different aspects of the batteries [13]. Furthermore, different test profiles also contain different test set-ups and parameters which can influence the accuracy that can be obtained from the ECM. Hence, choosing the correct test profile is key in obtaining the required measurements and accuracy of these measurements for the relevant battery parameters.

2.3.1 Dual Polarisation Model

As mentioned above, several different battery models can be used, according to [11, 12, 14]. The most simple model is the Rint Model (Figure 1a). This model consists of a single voltage source which represents the Open Circuit Voltage (OCV) as a function of the State of Charge (SoC) of the battery, and a resistor in series which represents the internal resistance of the battery as a function of the SoC [14]. Although this is a valid battery model, it is generally not accurate enough and it is unable to model many of the relevant parameters of a battery [14, 18]. A different model which can be used is the Thevenin Model. This model consists of the Rint model, but with an additional

in parallel resistor and capacitor (RC) pair in series with the resistor of the Rint model. In an ECM, according to [11,18], RC networks are used to simulate the electrical behavior of the battery without explicitly taking into account the internal mechanism inside the battery. This includes the physical and chemical properties of the positive and negative materials, the internal diffusion process of the battery, the electrochemical reaction process, etc. [11]. This additional RC pair in the Thevenin Model is able to portray the electrochemical polarisation within the battery [19]. Electrochemical polarisation, as explained in [19], refers to the polarisation phenomenon caused by the electrochemical reaction velocity on the positive and negative electrodes being less than the electron movement velocity in the battery. In order to model additional battery parameters and improve the accuracy of the ECM, more RC pairs need to be included [18]. This is the case in the Dual Polarisation Model (Figure 1b), which is similar to the Thevenin Model, but with an additional RC pair included. This additional RC pair is utilised to model another aspect of the electrochemical polarisation phenomenon [19]. In this case, the additional RC pair characterises the concentration difference polarisation of the battery [19]. This is defined as the diffusion rate of the battery in the solid phase, which is less than the electrochemical reaction rate when the battery is being used [19]. With this additional RC pair, as seen in Figure 2, more of the characteristics of the battery can be obtained [11,18].
The ECM used in this paper, namely a Dual Polarisation (DP) ECM, is illustrated below in Figure 2. There are a few reasons for this choice. To begin with, a lot of research and testing has already been conducted using this particular ECM, therefore making it easy to compare and verify the process with other research papers that have done similar tests. Secondly, as mentioned previously, increasing the number of RC pairs improves accuracy, but at a certain point the complexity outweighs the added accuracy. Due to this, a two RC pair ECM such as the Dual Polarisation Model is considered more than sufficient regarding complexity and accuracy. Lastly, the type of model is not the most important aspect of this paper, the HPPC testing combined with the Cascaded H-Bridge (CHB) is. Therefore, the focus has been on the process of testing and the parameter identification method rather than on the particular ECM chosen.

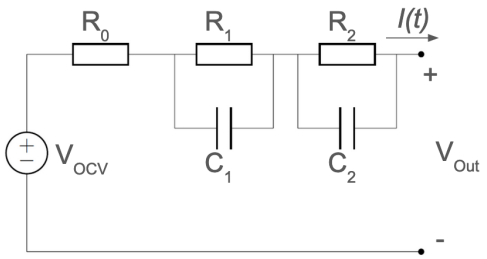

Figure 2: Dual Polarisation ECM for Battery [14]

2.3.2 Parameter Identification

To determine the circuit parameters (R_0, R_1, C_1, R_2, C_2) of the Dual Polarisation (DP) model, a Hybrid Power Pulse Characterisation (HPPC) test is conducted. This test consists of sending a varying current pulse through the DP ECM simulation, and with the data of the test, calculating the values of the circuit parameters.
An example of the current pulse used to determine the parameters of the DP ECM can be seen below in Figure 3. The goal of sending a varying current pulse through the circuit is to produce a voltage response graph, as seen in Figure 3. From the voltage graph, key points can be found which can be used to determine the DP ECM circuit parameters. As mentioned in section 1, the goal of this paper is to develop an online state of health estimation method using a cascaded H-Bridge for different State of Charges (SoC) of a battery. To do this, the current pulse seen in Figure 3 needs to be conducted for a range of State of Charges of the battery.

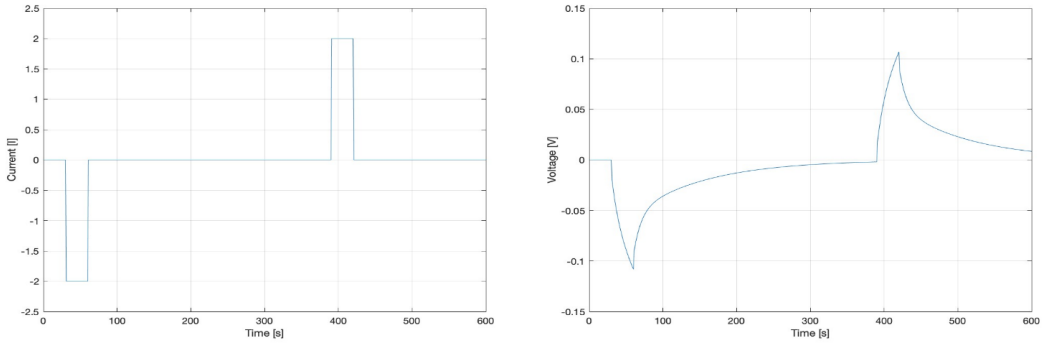

Figure 3: Ideal HPPC Current Input (left) and Ideal Voltage Response of DP ECM for HPPC Current Input (right)

To determine the equation for the battery output voltage, Kirchoff's voltage law can be applied to Figure 2. Defining the voltage V_{OCV} as the Open Circuit Voltage of the battery and V_1 and V_2 as the voltage across the RC pairs respectively, the following equation can be found.

$$V_{Out} = V_{OCV} - V_{R_0} - V_1 - V_2 \tag{3}$$

Where V_{R_0} is the voltage across the resistor R_0. Furthermore, due to the HPPC current input signal varying with time, the voltages over V_{R_0}, V_1, and V_2 also vary with time. This means that the equations that are needed to describe the voltages across the components will also be dependent on the time of the current within the circuit.
To determine the equations for the voltages V_{R_0}, V_1, and V_2, Kirchoff's voltage for each component can be used to derive the characteristic equations. These equations can be seen below [18, 20, 21].

$$V_{R_0} = I(t) \cdot R_0 \tag{4}$$

$$\frac{dV_1}{dt} = -\frac{V_1}{C_1 \cdot R_1} + \frac{I(t)}{C_1} \tag{5}$$

$$\frac{dV_2}{dt} = -\frac{V_2}{C_2 \cdot R_2} + \frac{I(t)}{C_2} \tag{6}$$

Where $I(t)$ is the current, R_0 is the internal resistance, R_1 and C_1 represent the electrochemical impedances, and R_2 and C_2 represent the polarisation impedances.
From Figure 3, it can be seen that the voltage response to the HPPC input current is exponential. This is because the equations for V_1 and V_2 can also be written in discrete time form. This is done for easier implementation later on when using data fitting models to estimate the parameter values. The discrete time equations can be seen below [11, 18–21].

$$V_1(t) = V_1(t-1) \cdot exp(-\frac{\Delta t}{\tau_1}) - R_1 \cdot I(t-1) \cdot exp(-\frac{\Delta t}{\tau_1}) \tag{7}$$

$$V_2(t) = V_2(t-1) \cdot exp(-\frac{\Delta t}{\tau_2}) - R_2 \cdot I(t-1) \cdot exp(-\frac{\Delta t}{\tau_2}) \tag{8}$$

Where Δt indicates the stepping size of the function, τ_1 is the time constant of the first RC pair, and τ_2 is the time constant of the second RC pair. The time constants can be calculated using the following equation, where n is the order of the RC pair.

$$\tau_n = R_n \cdot C_n \tag{9}$$

Using Equation 4, Equation 7 and Equation 8, the parameters values R_0, R_1, R_2, C_1, and C_2, can be estimated using a data fitting model script in MATLAB.

2.3.3 State of Charge Derivation

As outlined in 2.1 - 2.2, the estimation of the SoH requires the determination of the maximum capacity, $Q_{max}(t)$ of the battery at any point while it has been used. For this, the State of Charge also needs to be determined for the DP ECM. The equation for the SoC can be seen below [18, 20–22].

$$SoC = SoC(t) - \frac{\eta}{Q_n} \int I(t)dt \tag{10}$$

Where η is the coulombic efficiency of the battery, and Q_n represents the nominal battery capacity [18, 21]. Equation 10 describes the current SoC as a function of the initial SoC of the battery.
As with the voltages V_1 and V_2 in Equation 7 and Equation 8, the SoC equation has to be converted into a discrete time equation to simplify the integration with the MATLAB script. The discrete time SoC equation can be seen below [18–20].

$$SoC(t) = SoC(t_0) - \frac{\eta}{Q_n} \cdot \Delta t \cdot I(t-1) \tag{11}$$

Where, similar to the discrete equations for V_1 and V_2, the Δt is the stepping size of the function.

2.4 Hybrid Power Pulse Characterisation

Hybrid Power Pulse Characterization (HPPC) is a model-based ('online') estimation method that consists of alternating sending short square wave signals and relaxation periods that charge and discharge the battery [16]. By alternating sending signals and charging/discharging the battery, a constant State of Charge (SoC) of the battery can be obtained. This is crucial to limit the change in parameter values for different SoC values. Through HPPC, an analysis of the power capability of the battery is conducted under different conditions [23]. These conditions can be: charge and discharge, current rate, ambient temperature and State of Charge (SoC) [23]. By investigating the battery under these different conditions, a better understanding of how the battery operates can be obtained.
The general concept of HPPC, as outlined in [24], consists of having a battery in a steady-state before the battery is pulsed with charging and discharging currents. In this context, steady-state refers to the battery being charged to a specific State of Charge before allowing it to rest to ensure that the battery temperature does not affect the results. The battery is then pulsed with a varying current pulse and then left to rest to return to the initial SoC of the test. Furthermore, the battery is monitored using voltage and current sensors which record the response of the battery to the HPPC signal. With the current and voltage measurements, data fitting models can be used to determine the battery parameters R_0, R_1, R_2, C_1, and C_2.
To determine the parameters of the HPPC test, pulse length, pulse rest, and pulse height need to be considered. According to [11], two parameters that can affect the accuracy of the ECM with HPPC as a method of testing are the length of the pulse and the height of the positive pulse. It was deduced that a shorter pulse produced a higher simulation accuracy [11]. Therefore, in this paper, 20 seconds were used for pulse lengths. Furthermore, the pulse length also has an effect on the accuracy of the simulation [11, 12]. As stated in [12], the length of time after the pulse should be much longer than the time constants (τ_1 and τ_2) of the battery model. This ensures that the battery has enough time to stabilize before the next pulse [12]. Lastly, pulse height refers to the current used in the HPPC test. In standard HPPC practice, positive and negative pulses have varied C-rates, as outlined in [11, 24]. C-rates are defined as the charge/discharge current rate of the battery divided by the nominal battery capacity [25]. Many research papers do have varied C-rates for charging and discharging pulses, although this is not always the case as seen in [23]. This is due to running tests/simulations in which the SoC is varied, which can be achieved by having the negative pulse have a larger C-rate to draw more current. In this paper, the SoC is maintained constant, therefore the pulse height for both positive and negative pulses is kept equal.

2.5 Data Fitting Model

To be able to extract the parameter values of the ECM from the HPPC test, a Data Fitting Model (DFM) is needed. DFM's are algorithms that can be used to determine parameters from gathered output data. There are many types of data fitting models that can be used. Examples of data fitting models are the recursive least squares (RLS) model [18], the particle swarm optimization (PSO) model [13], and exponential curve fitting (ECF) [26]. Different data fitting models have different degrees of accuracy depending on the constraints and complexity of battery ECM used. The goal of the data fitting models is to extrapolate relevant values of data from a test, and to try to correlate the values with known initial values. The better the correlation between the test values and the known initial values, the more accurate the battery test can be considered.
The data fitting model used in this paper is from the MATLAB Optimization Toolbox, more specifically *gamultiobj* [27]. This particular MATLAB function that uses a Pareto front to set the variables into a parameter space, and then evaluates each variable to find the set of parameter values with the most likeness to the simulated output [27]. By giving the DP ECM initial values and varying the OCV value, the function then calculates the values of the different components based on voltage output response.

2.6 Cascaded H-Bridge

As mentioned in the Introduction, the aim of this paper is to create an online method for battery State of Health (SoH) estimation using a Cascaded H-Bridge (CHB). An overview of the CHB is illustrated below in Figure 4.

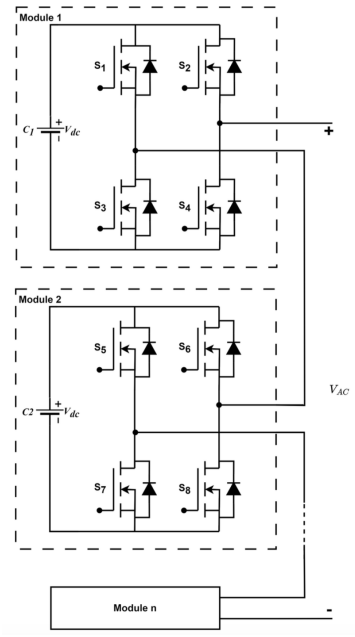

Figure 4: Overview of Cascaded H-Bridge Integrated with Battery Modules [2, 28]

The main function of an H-Bridge is to be able to change the polarity of the initial voltage signal by changing the configuration of the MOSFETs. The Cascaded H-Bridge (CHB), shown in the figure above, is comprised of two sets of four MOSFETs. From the configuration of the MOSFETs, it can be seen that there are four basic states in an H-Bridge [2, 28]. These states are namely: P, N, Z_1, and Z_2, where the outputs are $+V_{DC}$, $-V_{DC}$, and zero respectively [2, 28]. An overview of the different MOSFET configurations is illustrated below in Figure 5.

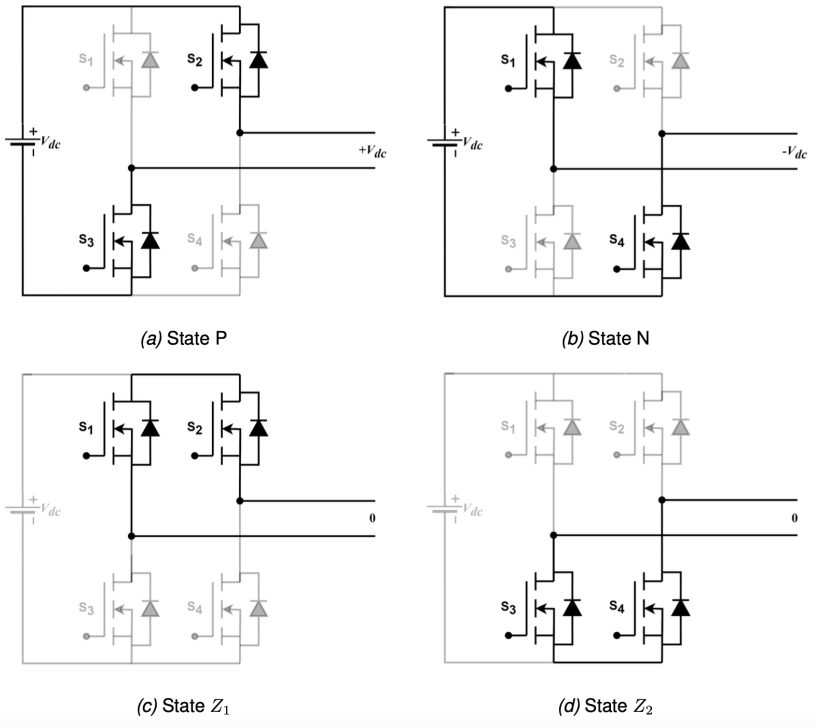

Figure 5: Possible MOSFET Configurations in an H-Bridge [2]

The advantage of using HPPC as a testing procedure for battery state of health estimation is that it can be combined with a cascaded H-Bridge. As outlined in [16] and [29], sending positive and negative currents allows for the voltage response of the system to be determined. Due to the structure of a CHB, input voltages can be varied by switching different MOSFET pairs to power other components. For example, looking at Figure 5, if MOSFETs S_2 and S_3 are activated then a positive voltage can be measured across the output of the H-Bridge. On the other hand, MOSFETs S_1 and S_4 can be activated to be able to measure a negative output across the H-Bridge. To rest the battery between the tests, then either MOSFET pairs S_1 and S_2 or S_3 and S_4 can be activated.

Furthermore, the advantage of using a Cascaded H-Bridge (CHB) is that the speed of the state switching can be varied. This allows for the CHB to be used for different input frequencies and for different amounts of time.

A Cascaded H-Bridge would be used for multiple arrays of batteries, but due to simulating a singular battery, a single H-Bridge will be used instead.

Furthermore, the input of the cascaded H-Bridge will not be a constant DC voltage source, as seen in Figure 5, but an AC voltage source. An AC voltage source is used instead of a DC voltage source to mimic the H-Bridge connection to a power grid, such as a connection to an outlet in a house. This means that the layout of the H-Bridge will be slightly different, as illustrated in Figure 6, but the working principle stays the same.

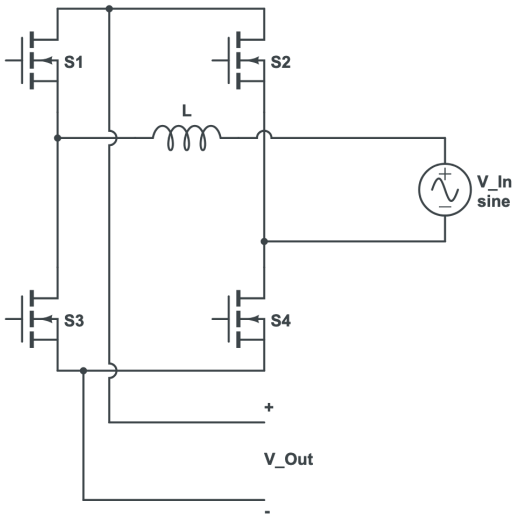

Figure 6: AC Input Signal H-Bridge Configuration

The advantage of using an AC voltage source is that due to the possible MOSFET configurations, the sinusoidal input can be manipulated to output a DC voltage source. This is achieved by timing the switching of the MOSFET pairs to mimic the sign of the sinusoidal input, creating what is known as a full wave rectifier [30–33]. An example of the output of the full wave rectifier and the initial sinusoidal input is illustrated below in Figure 7.

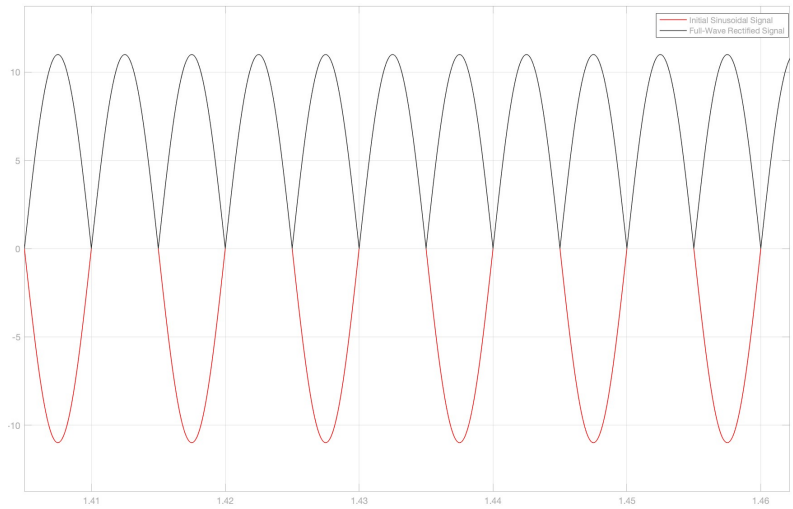

Figure 7: Comparison of Initial Sinusoidal Signal and Full Wave Rectified Signal

To control the switching of the MOSFETs in the H-Bridge to ensure that the AC voltage is fully rectified, a voltage PI controller is needed. The goal of the PI controller is to regulate the voltage link between the H-Bridge and the Bi-Directional converter. The PI controller is illustrated below in Figure 8.

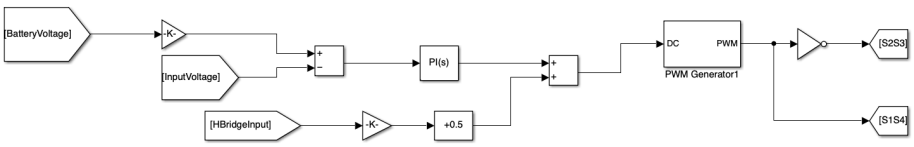

Figure 8: H-Bridge PI Controller Schematic

The PI controller receives the calculated voltage error between the battery voltage and the DC voltage input of the converter circuit. The controller output is then scaled with the duty cycle of the initial H-Bridge AC voltage before being converted into a Pulse Width Modulated (PWM) signal. This signal is then split, and sent to the two different MOSFET configurations $S_1\&S_4$ and $S_2\&S_3$.
The full wave rectified signal can then be filtered, using a low-pass Pi filter to create a constant DC voltage [34]. By filtering the full wave rectified signal, there is some voltage loss [30–33]. Therefore, a higher initial AC voltage is needed to ensure that the Bi-Directional DC-DC Buck-Boost Converter has enough input voltage to operate correctly. The relation between input voltage and output voltage of the full wave rectifier is described in the equation below [31].

$$V_{DC} = \frac{2 \cdot V_{max}}{\pi} = 0.637 \cdot V_{max} \tag{12}$$

Where V_{max} is the maximum voltage of the sinusoidal input voltage, and V_{DC} is the DC output voltage value. By setting the desired V_{DC} value, the equation can be rearranged to calculate the initial sinusoidal voltage input needed.
The Pi filter for the H-Bridge is illustrated below in Figure 9. A Pi filter is used to smooth the full wave rectified output due to its low ripple factor and high voltage output [34].

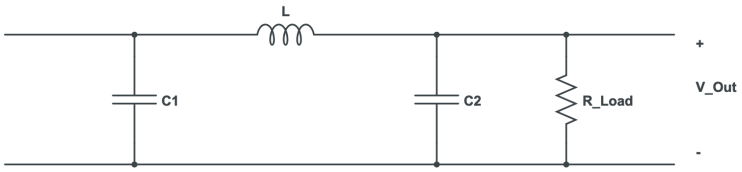

Figure 9: H-Bridge Filter Model

As can be seen in the figure above, the Pi filter consists of two capacitors separated by an inductor. The first capacitor in the filter provides a low resistance to the AC ripple and a high resistance to the underlying DC voltage [34–36]. The filtered signal passes through the inductor, which provides low resistance to the DC voltage while amplifying any remaining AC ripple in the signal [34–36]. The second capacitor further filters the remaining AC ripple, leaving only the DC component of the signal [34–36]. This is then used as the reference voltage of the Bi-directional DC-DC converter.
To determine the values for the components in the Pi filter, the following equation is used [37].

$$f_c = \frac{1}{2\pi\sqrt{LC}} \tag{13}$$

Where f_c is the cut-off frequency, C is the capacitance value, and L is the inductor value. By determining the desired cut-off frequency, of the input signal and setting one of the parameter values, the remaining parameter value can be calculated.

2.7 Bi-Directional DC-DC Buck Boost Converter Circuit

To implement the H-Bridge for HPPC testing, a small converter circuit is needed. In this case, the circuit needed is a Bi-Directional DC-DC converter [29, 38]. This circuit is illustrated below in Figure 10.

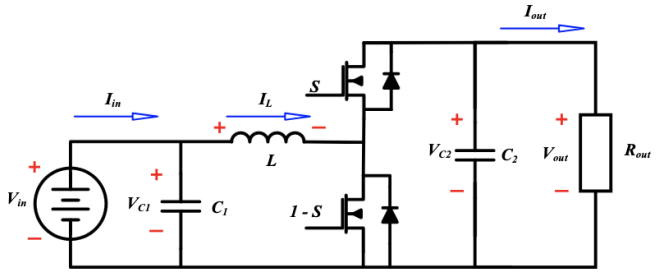

Figure 10: Bi-Directional DC DC Buck Boost Converter [29, 38]

The goal of this circuit is to provide an up or down voltage conversion between the battery and the reference voltage, as well as a switching mechanism for the HPPC signal. Due to the structure of the Bi-Directional DC-DC Buck-Boost Converter, the circuit can vary how it reacts to different voltages across V_{out} by switching the gates of the two MOSFETs. To determine the necessary input voltage as the reference voltage of the circuit, the following equation can be used [39].

$$V_{DC} = \frac{V_{battery}}{1 - D} \tag{14}$$

Where V_{DC} is the input reference voltage, $V_{battery}$ is the battery voltage, and D is the value of the duty-cycle which varies between 0 and 1. By determining the voltage of the battery at a point in time, the reference voltage can be determined using the equation stated above.
As mentioned above, this circuit is also used due to the inductor, which is used as a current storage element, and as a voltage controlled current source during different state of operation. Furthermore, the inductor also reduces ripples and smooths signals within the converter.
To find the value of the inductor in the Bi-directional converter, the two state of the converter needs to be taken into account. Due to V_{DC} being larger then $V_{battery}$, the converter works mostly in buck mode. Therefore, the value of the inductance value can be calculated using the buck mode equation [40].

$$L = \frac{D}{2 \cdot I_o \cdot f_s} \cdot (V_{DC} - V_{battery}) \tag{15}$$

Where L is the value of the inductance, D is the value of the duty cycle, I_o is the current value, f_s is the switching frequency, V_{DC} is the value of the DC voltage link between the H-Bridge and the converter, and $V_{battery}$ is the voltage of the battery.
The timing of the MOSFET switches is done using a Proportional-Integral (PI) Controller. The controller set-up is illustrated below in Figure 11.

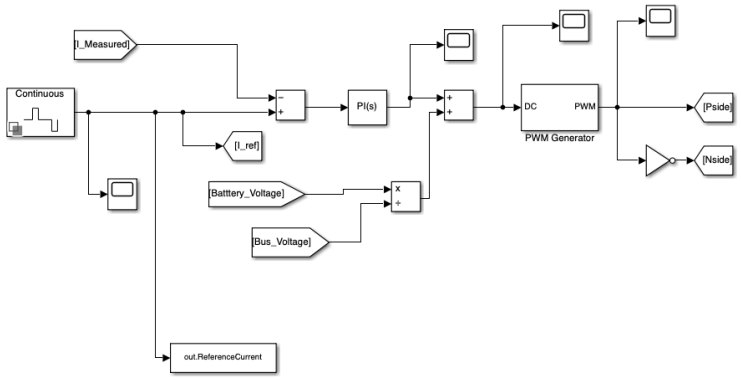

Figure 11: Bi-directional Converter PI Controller Schematic

The idea behind the PI Controller is to be able to sense changes in the measured current of the Bi-directional converter and to be able to adapt the switching of the MOSFETs to match with the desired signal input [38]. In this case, the desired signal input is the HPPC signal, seen on the right in Figure 3. This input is compared to the measured output of the circuit, which is sent to the PI controller to create a controller signal. From the PI controller, the signal is then summed with the duty ratio of the MOSFETs. The equation can be seen below [41–43].

$$D = \frac{V_{battery}}{V_{DC}} \tag{16}$$

Where D is the duty ratio, $V_{battery}$ is the voltage across the battery and V_{DC} is the input DC voltage of the converter. The sum of the PI output and the duty cycle is done to scale the output of the PI controller. This ensures that the output of the PI controller matches the required duty cycle of the system. This signal is then compared to a saw-tooth wave to create the Pulse Width Modulated signal. The PWM signal is then sent to the MOSFETs, which drives the switching of the gates in the circuit. To ensure that the MOSFETs are not powered at the same time, which would cause a short circuit, one of the MOSFETs has an inverted input. This ensures that the gates are on at alternating intervals.

3 Methodology

3.1 Battery

The battery used in this paper is a Sanyo NCR18650GA Li-ion battery cell [25, 29]. This battery is a high energy 18650-type battery cell, with a total capacity of 3350 mAh, a maximum discharge current of 10 A and a voltage range between 2.5 and 4.2 V [25, 29].

3.2 Dual Polarisation Equivalent Circuit Model Parameter Derivation

To be able to conduct testing, the Dual Polarisation ECM needs to be constructed. This was done in Simulink, a simulation program from MATLAB [6]. The Dual Polarisation model can be seen below in Figure 12.

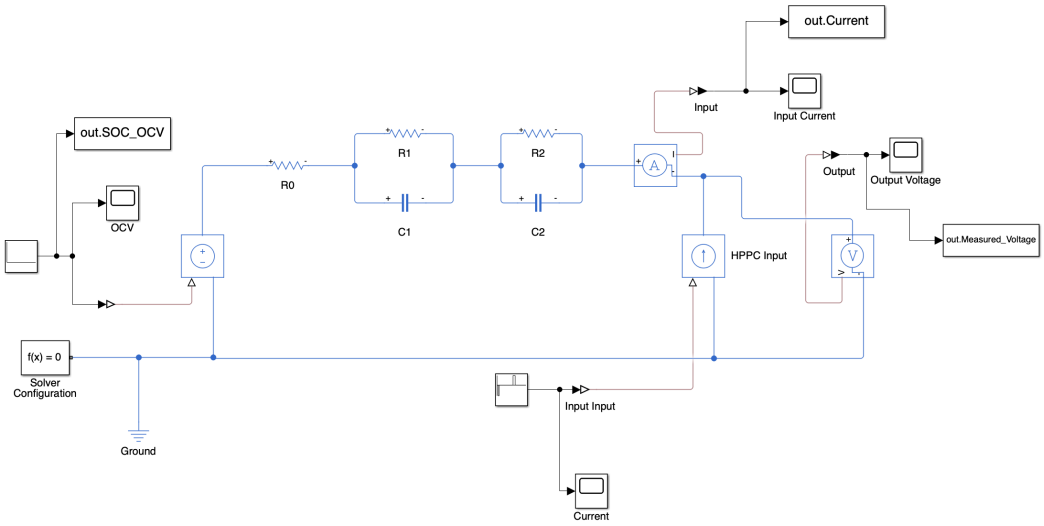

Figure 12: Simulink Dual Polarisation ECM

Similar to the model seen in Figure 2, the DP ECM in Figure 12 consists of a voltage source that represents the Open Circuit Voltage (OCV), the resistor R_0 which is the internal resistance of the battery, and the two RC pairs. The initial values of the parameters are derived from [29]. An overview of the values is given below in Table 1.

Table 1: Initial Parameter Values

Parameter	Initial Values
V_{OCV}	$3.55[V]$
R_0	$0.0473[\Omega]$
R_1	$0.0340[\Omega]$
R_2	$0.0283[\Omega]$
C_1	$0.637[F]$
C_2	$641[F]$

To conduct the HPPC testing, a controlled current source, located on right side of the ECM, is used. This source block sends a varied signal which represents the current drawing and sending current to the battery.
To determine the parameter values for different voltages, the OCV is changed within a defined range, in this case between zero and five volts. The data from these simulations is then gathered,

and through the use of data fitting models available in MATLAB, the parameter values are extracted from the data.
Having extracted the parameter values for independent OCV values, the circuit can be modified to work for varying OCV inputs. The Simulink circuit model can be seen below in Figure 13.

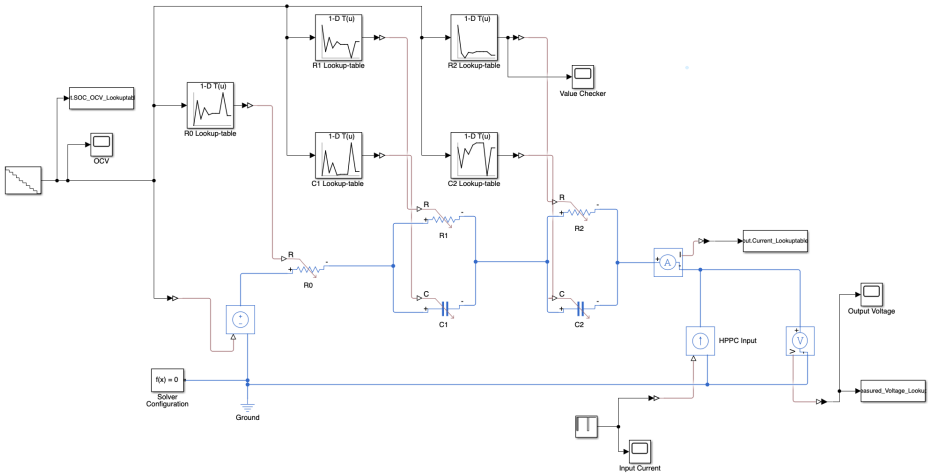

Figure 13: Simulink Dual Polarisation ECM with Variable Components and Lookup Tables

The new model consists of variable components, which can receive the correct resistance or capacitance values from their respective lookup tables, based on the input voltage of the OCV. Lookup tables are used to speed up the simulation process as they mitigate the need to calculate parameter values for different input voltages. Furthermore, within the lookup tables, values between measured voltages can be interpolated, further reducing the amount of initial simulations needed to gather circuit parameter values. The estimated parameter values are given in Table 2, in subsection 7.2.

3.3 State of Charge

To derive the State of Charge of the circuit, Equation 10 is used as a basis. Using the Simulink blocks, as seen in Figure 14, Equation 10 can be reconstructed to calculate the SoC while the simulation is running. The continuous equation is used instead of the discrete one as integrating while the simulation is running ensures no discontinuities are introduced.

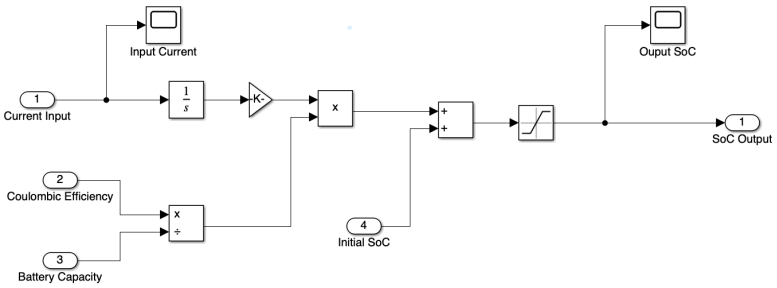

Figure 14: SoC Calculation Circuit

The output of the calculation is then fed back into the dual polarisation model to help determine the values for the components from the lookup tables. This ensures that the values change accordingly to the voltage of the circuit.

3.4 Hybrid Power Pulse Characterisation Test Set-up

To conduct an HPPC test, an input signal needs to be designed. The goal of the input signal is to vary the state of the charge of the battery by either charging or discharging the battery with current pulses. From the data collected from these tests, the parameters within the model can be computed for the changing circuit parameters.
An example of the input current and the expected voltage response of the DP ECM are illustrated in Figure 3. The input current pulses are created using the H-Bridge and the Bi-Directional Dc-DC Buck-Boost Converter. A value of 2 ampere was chosen as for the HPPC current pulses. This specific current value, which translates to 0.6 C-rate of the battery, is used as it is equivalent to one-fifth of the maximum discharge of the battery [25]. This represents a moderate charge and discharge rate for the battery [44]. In practice, as mentioned earlier, the standard HPPC practice uses different C-rates for charging and discharging rates. The common C-rate values seen in many research papers such as [11], and outlined in [24], are $0.75C$ for charging and $1C$ for discharging. Furthermore, in [11], broader C-rates were also tested to see the effectiveness of different parameters on the accuracy of ECMs. Based on this, a C-rate of $0.6C$ was chosen.

3.5 Data Fitting Model Selection

Within MATLAB, there are many toolboxes that can be used for parameter identification. In this case, the Optimization Toolbox is used to determine the parameters. By extracting the current, voltage, and OCV from the simulation, and defining the equations for the two RC pairs, the Optimization toolbox is able to find the best values for the individual parameter components.
To ensure that the component values are non-zero, upper and lower boundaries are set. For this paper, the maximum boundary for each component is the value of each component presented in Table 1. The lower boundary is one-tenth of the upper limit. This ensures that a large range of values can be used by the Optimization script to find the best values. Furthermore, these boundaries are set with these limits as the expected parameter values should be within range of previously estimated parameter values.
Within the Optimization toolbox, for data fitting the function *gamultiobj* was used [27]. This was the recommended option in the Optimization Toolbox for multi-variable optimization. Furthermore, inserting Equation 3, Equation 4 Equation 7, Equation 8 into the script, and defining the boundaries for all variables allowed for the optimized parameters to be estimated. From the results of the optimized parameters, a separate MATLAB script was used to find the lowest value for each parameter. The lowest value is used due to how the MATLAB *gamultiobj* function works. The function creates a Pareto front, which searches for the lowest values that satisfy the requirements set in the optimization script [27]. These values were subsequently used for calculating the voltage response of the circuit for different OCV values.

3.6 H-Bridge and Bi-Directional Converter Circuit

As with the DP ECM, mentioned previously, the combined H-Bridge and Bi-Directional DC-DC Buck-Boost Converter circuit also needs to be implemented into Simulink to be able to conduct testing. The circuit schematic is illustrated below in Figure 15

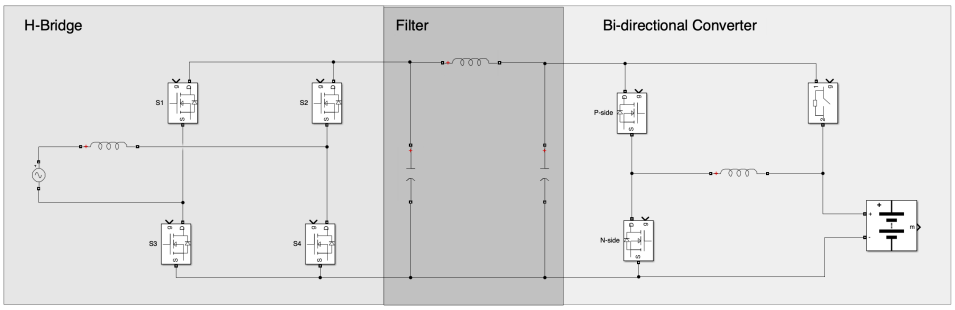

Figure 15: Circuit Schematic of H-Bridge and Bi-Directional Converter

The Simulink model for the combined circuit can be seen below in Figure 16.

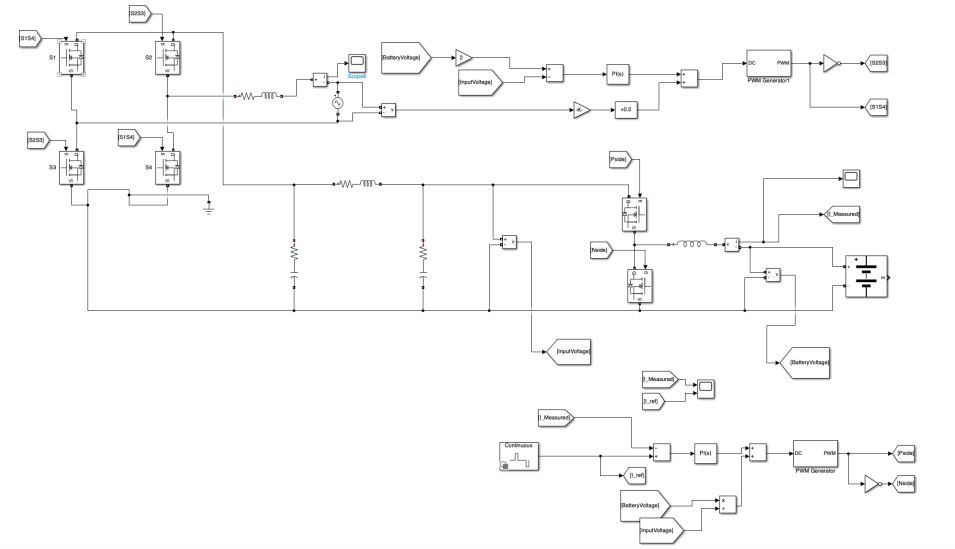

Figure 16: Simulink H-Bridge and Bi-Directional DC-DC Buck-Boost Converter

The individual circuits for the H-Bridge and the Bi-Directional DC-DC Buck-Boost Converter is illustrated below in Figure 17 and Figure 18

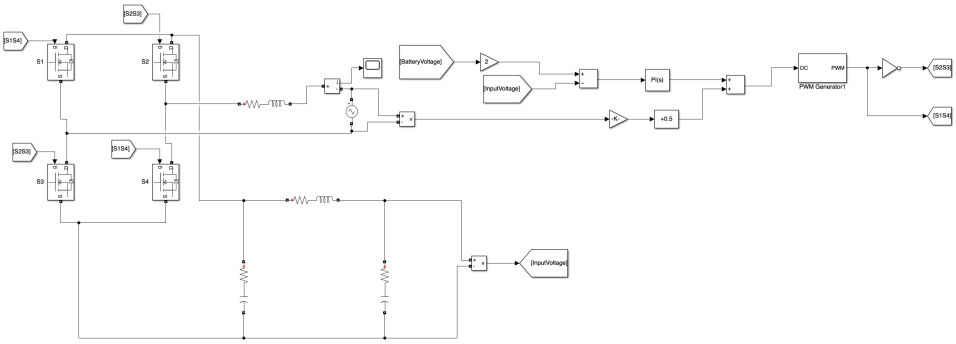

Figure 17: Simulink H-Bridge Circuit

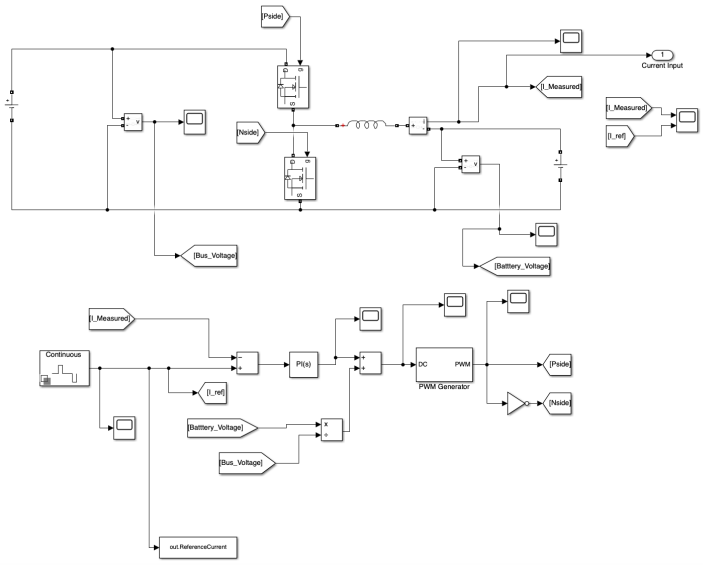

Figure 18: Simulink Bi-Directional DC-DC Buck-Boost Converter Circuit

The entire circuit is illustrated below in Figure 19.

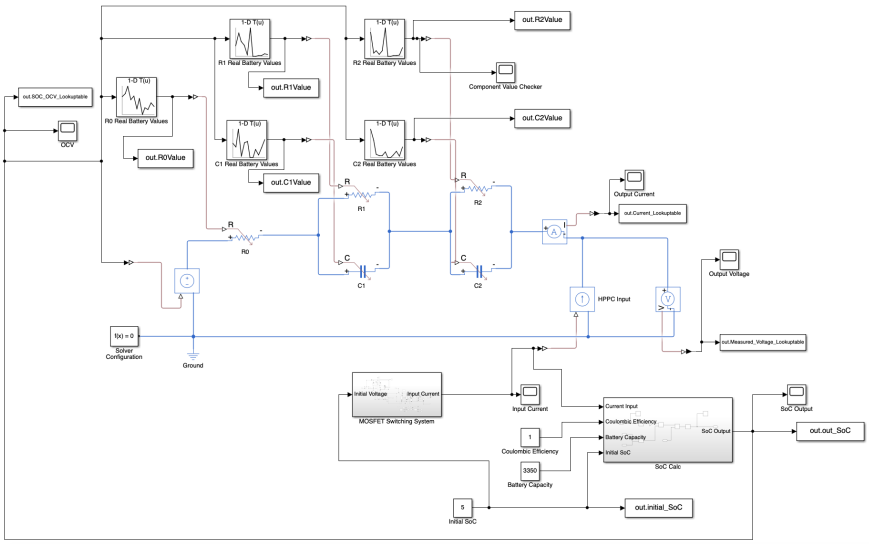

Figure 19: Entire Simunlink Model

Combining the three separate circuits, along with the SoC calculation block, the model is able to adapt to different OCV input values. By using a H-Bridge and Bi-Directional DC-DC Buck-Boost Converter, the initial OCV can be manipulated to test the battery at different voltage values.
Due to the high voltage used as the input of the converter circuit, the set-up of the complete model is slightly different from the initial DP ECM model. In the complete circuit model, it is assumed that an array of batteries is used instead of a singular low-voltage battery. Therefore, ten batteries in series are used to ensure that the operating voltage of the controller matches the maximum input voltage of the batteries. It is also assumed that the batteries all have the same internal component values. This means that the initial parameters derived need to be adjusted to fit the model. In this case, the resistances R_0, R_1, and R_2 are multiplied by ten, and the capacitances C_1, and C_2 are divided by ten.

4 Results

In the following sections, the results of the two circuits, the initial DP ECM and the complete DP ECM with the Bi-Directional converter circuit and H-Bridge, will be presented. To begin with, the results of the initial Dual Polarisation Model, illustrated in Figure 12 will be presented. This includes the parameter values obtained from the MATLAB Optimization Toolbox and the voltage response graphs. Following this section, the results of the complete Dual Polarisation Model, as illustrated in Figure 19 will be presented. This includes graphs showing the parameter values obtained from simulations, the voltage response graphs, and the SoC graphs for the different OCV values. Lastly, the HPPC output graphs of the Bi-directional converter and the DC output voltage of the H-Bridge will be presented.

4.1 Initial Dual Polarisation Model Results

4.1.1 Estimated Parameter Values

Using the initial values from [29], summarized in Table 1, the estimated parameter values for a range of OCV values are derived. The estimated Dual Polarisation parameter values are illustrated below in Figure 20, Figure 21, Figure 22, Figure 23, and Figure 24. Furthermore, Table 2, found in subsection 7.2, states all values presented in the following graphs.

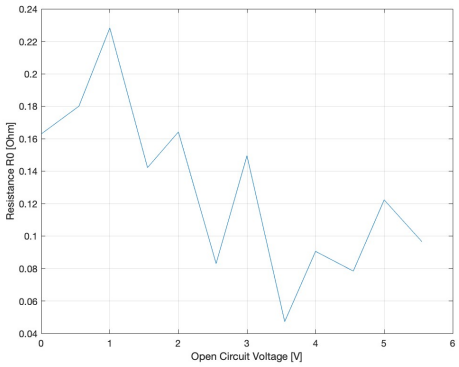

Figure 20: Estimated R_0 Values versus V_{OCV}

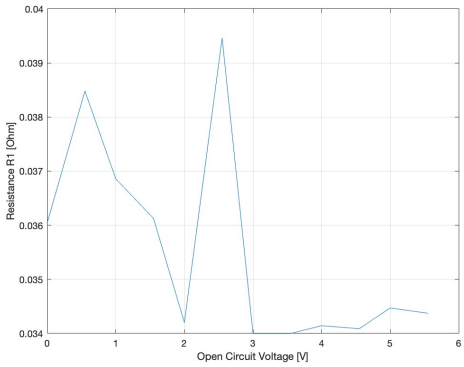

Figure 21: Estimated R_1 Values versus V_{OCV}

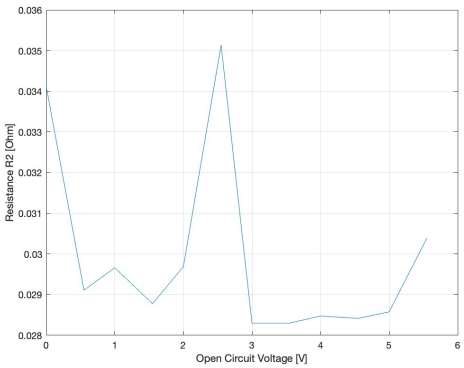

Figure 22: Estimated R_2 Values versus V_{OCV}

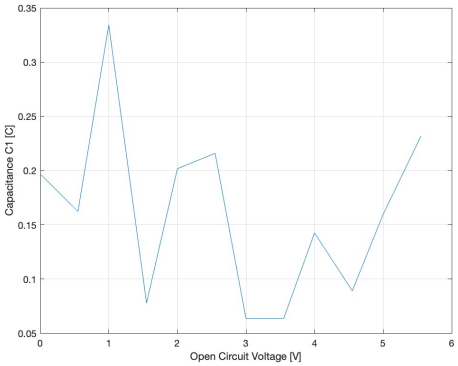

Figure 23: Estimated C_1 Values versus V_{OCV}

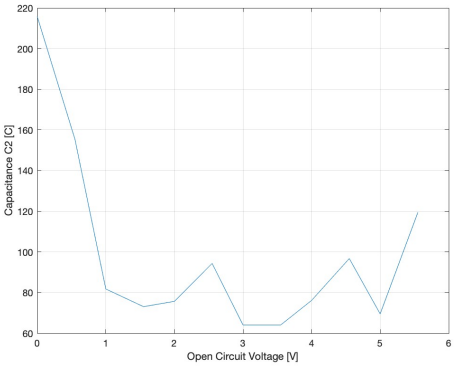

Figure 24: Estimated C_2 Values versus V_{OCV}

4.1.2 Voltage Response

To determine the validity of the estimated parameters, shown above, the voltage response of the circuit for different OCV values can be observed. The following graph, Figure 25, shows the voltage responses of the circuit with an OCV value of 2.55V.

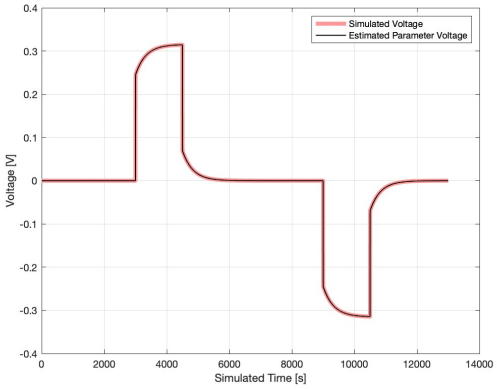

Figure 25: Voltage Response of Dual Polarisation Equivalent Circuit Model for Input Voltage of 2.55V

In the figure, the simulated voltage response, the red curve, and the estimated parameter voltage response, the black curve are shown. The simulated voltage response is the output of the Dual Polarisation ECM simulation, while the estimated parameter voltage is the calculated voltage response using Equation 7 and Equation 8. As illustrated in the figure, the calculated output overlaps the simulated output, indicating a high correlation between the values used in the model and the values derived using the data-fitting model.
The following graph, Figure 26, shows the voltage error between the simulated voltage of the circuit, and the calculated voltage using the parameter values corresponding to the initial 2.55V.

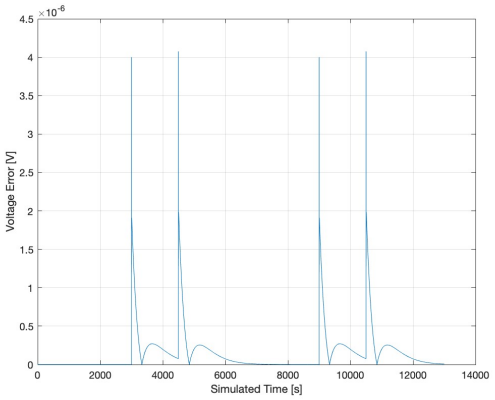

Figure 26: Voltage Response Error of Simulated Voltage Response and Calculated Voltage Response for Input Voltage of 2.55V

Similar to the parameter estimations, this is conducted across the 0 to 5.55 V OCV range. The graphs for the voltage response and error for the other OCV values can be found in subsection 7.3.

4.2 Complete Dual Polarisation Model Results

4.2.1 Estimated Parameter Values

Using the estimated parameters from the initial Dual Polarisation Model, the parameter values from the complete model were derived using the MATLAB Optimization script. The range of the estimated parameters is from 25.5 - 50V, which is ten times the operating voltage of the battery modelled in this paper. The values are then adjusted, using the impedance laws of resistors and capacitors, to model a single battery instead of the array of ten batteries in series. This is done to be able to compare the values from this simulation to the initial circuit simulation shown above in subsection 4.1. The graphs with the estimated values of R_0, R_1, R_2, C_1, and C_2 can be seen below in Figure 27, Figure 28, Figure 29, Figure 30, and Figure 31 respectively. The values are also summarized in Table 3, in subsection 7.4.

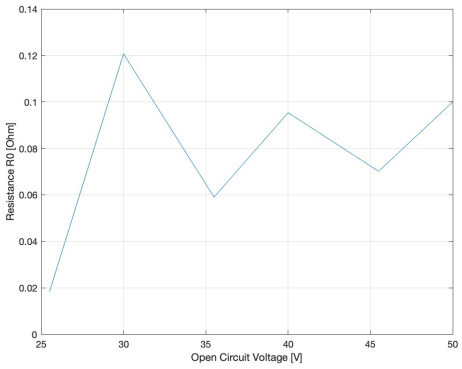

Figure 27: Estimated R_0 Values from Complete Circuit Model versus V_{OCV}

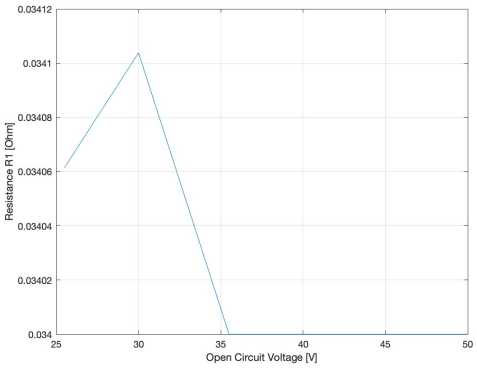

Figure 28: Estimated R_1 Values from Complete Circuit Model versus V_{OCV}

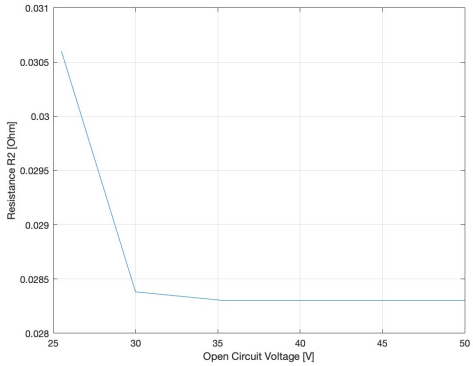

Figure 29: Estimated R_2 Values from Complete Circuit Model versus V_{OCV}

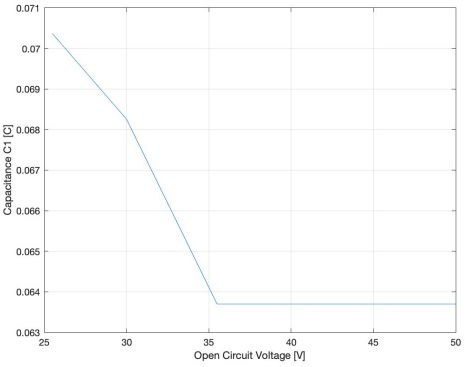

Figure 30: Estimated C_1 Values from Complete Circuit Model versus V_{OCV}

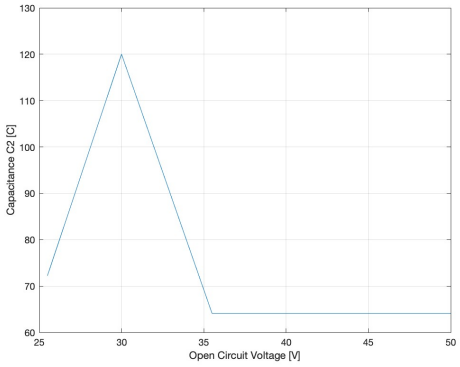

Figure 31: Estimated C_2 Values from Complete Circuit Model versus V_{OCV}

In the following figures, the parameter values obtained from the simulation through the use of the lookup-table for an initial OCV value of 25.5V are plotted. The graphs are illustrated below in Figure 32, Figure 33, Figure 34, Figure 35, and Figure 36.

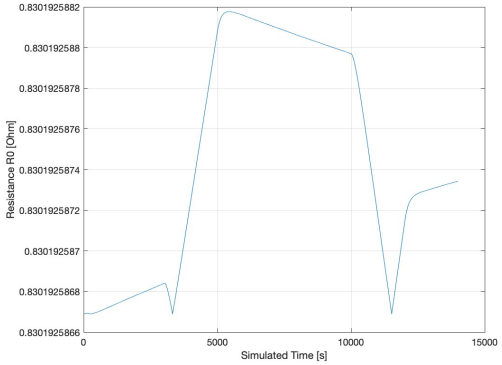

Figure 32: Simulated R_0 Values from Complete Circuit Model Lookup Table

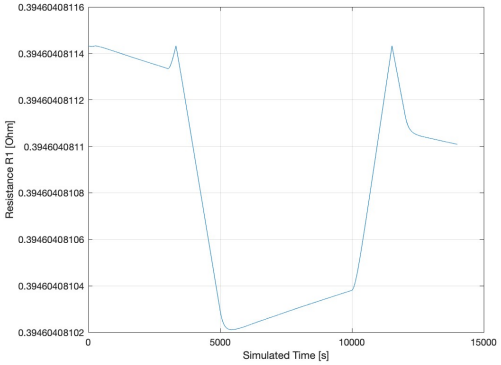

Figure 33: Simulated R_1 Values from Complete Circuit Model Lookup Table

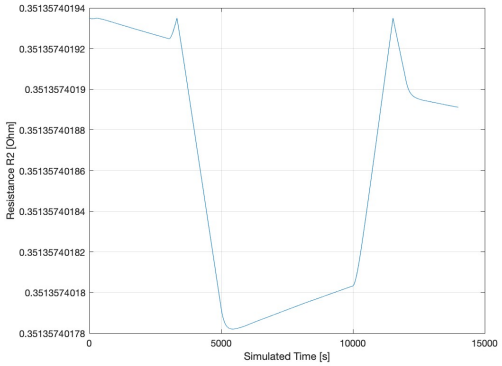

Figure 34: Simulated R_2 Values from Complete Circuit Model Lookup Table

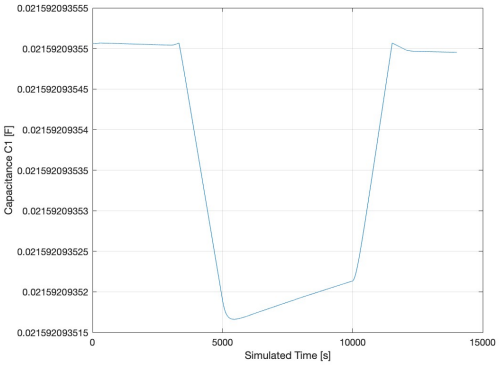

Figure 35: Simulated C_1 Values from Complete Circuit Model Lookup Table

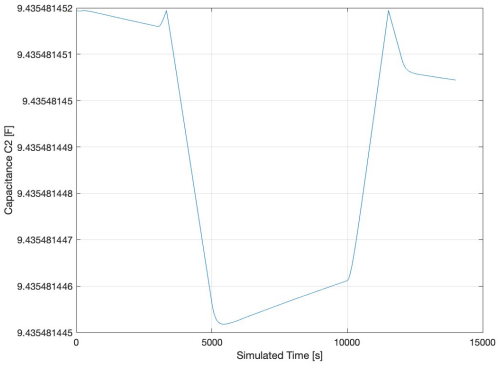

Figure 36: Simulated C_2 Values from Complete Circuit Model Lookup Table

4.2.2 Voltage Response

The voltage response of the complete circuit for different OCV values are plotted. The following graph, Figure 37, shows the voltage response of the circuit with an initial OCV value of 25.5 V.

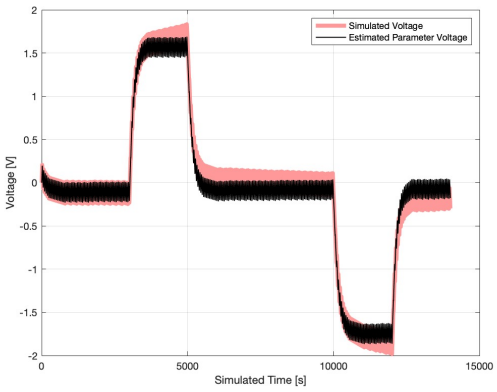

Figure 37: Voltage Response of Complete Circuit with Initial V_{OCV} Value of 25.5V

In the figure, the simulated voltage response of the complete circuit, plotted in red, along with the estimated parameter voltage response, plotted in black, are shown. Similar to the procedure stated in subsubsection 4.1.2, the estimated parameter voltage is calculated using Equation 7 and Equation 8.
The following graph, Figure 38, shows the voltage error between the simulated voltage of the circuit and the calculated voltage using the parameter values corresponding to the initial OCV value of 25.5 V.

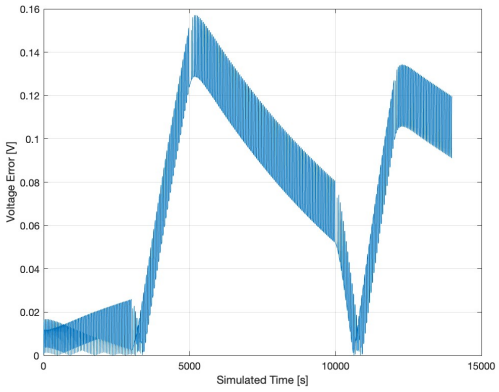

Figure 38: Voltage Response Error of Simulated Voltage Response and Calculated Voltage Response for Input V_{OCV} of 25.5V

The voltage response for the other OCV values are presented in subsubsection 7.4.1.

4.2.3 State of Charge

To determine the effects of the H-Bridge and the Bi-Directional DC-DC Buck-Boost Converter circuit on the Dual Polarisation ECM, the State of Charge (SoC) for the different OCV values can be plotted. The graph below, Figure 39, shows the Open Circuit Voltage (OCV) for an initial OCV value of 25.5V.

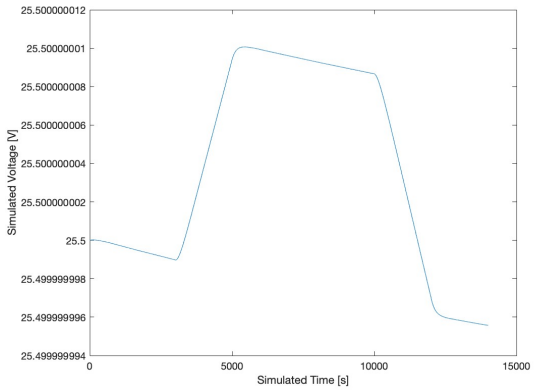

Figure 39: Calculated OCV of the Complete Circuit for an Initial OCV Value of 25.5V

This graph can be compared to the simulated OCV from the complete circuit simulation. The OCV from the complete circuit can be seen below in Figure 40, and the OCV error between the calculated and the simulated SoC can be seen in Figure 41.

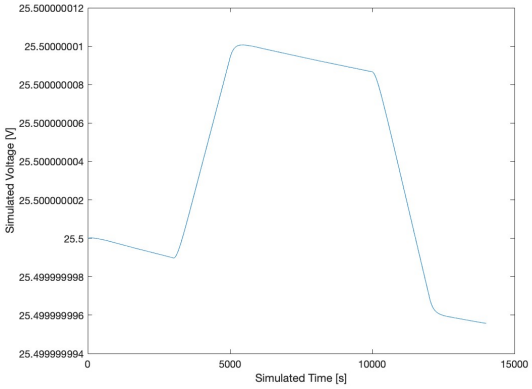

Figure 40: Simulated OCV of the Complete Circuit for an Initial OCV Value of 25.5V

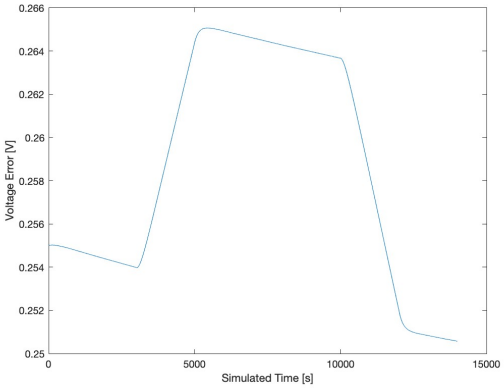

Figure 41: Error of the Complete Circuit OCV and the Simulated OCV for an Initial OCV Value of 25.5V

4.2.4 Current Graphs from Bi-Directional Converter

To verify the output of the Bi-Directional converter, the HPPC current output can be compared to the reference HPPC current input. The two HPPC current graphs can be seen in Figure 42, with the input curve plotted in red and the output curve plotted in blue.

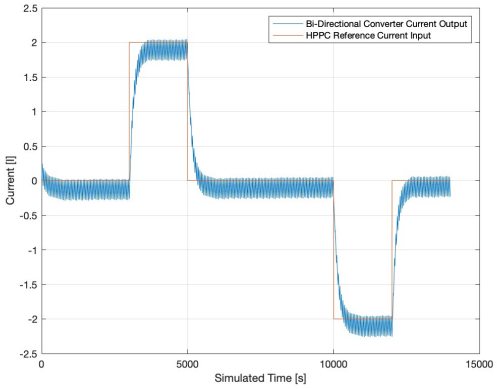

Figure 42: HPPC Current Comparison Between Bi-Directional Converter Current Output and Reference HPPC Signal

In the graph below, Figure 43, the calculated error between the two signals in Figure 42 is illustrated.

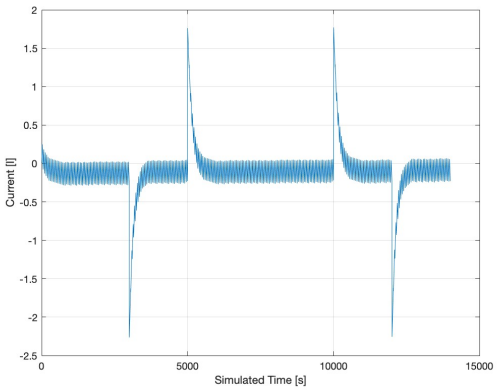

Figure 43: HPPC Current Error Between Bi-Directional Converter Current Output and Reference HPPC Signal

4.2.5 DC Voltage Graph of H-Bridge

To verify if the DC voltage link between the H-Bridge and the Bi-directional converter is stable, the voltage output can be graphed. This is illustrated below in Figure 44.

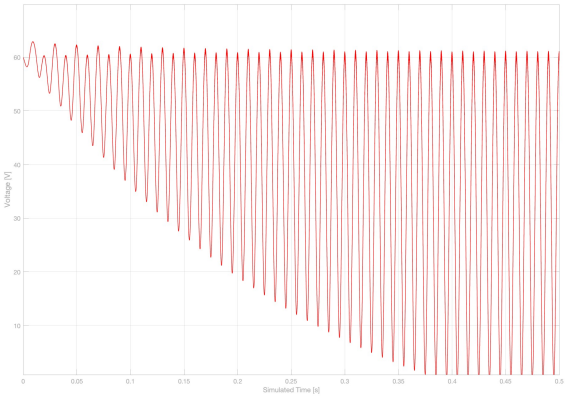

Figure 44: H-Bridge DC Voltage Output

4.3 ECM Parameter Value Comparison

To view the error between the estimated parameters of the initial DP ECM and the complete DP ECM, which includes the Bi-Directional converter, can be plotted. The graphs for the battery parameters R_0, R_1, R_2, C_1, and C_2 are illustrated in Figure 45, Figure 46, Figure 47, Figure 48, Figure 49 respectively.

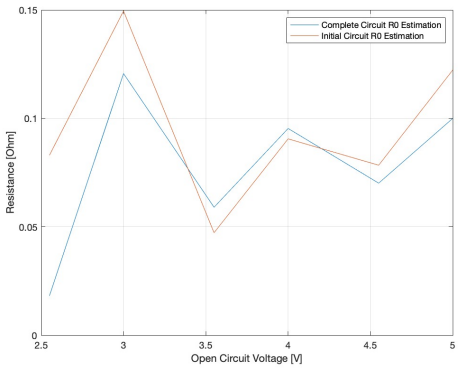

Figure 45: Graph with Comparison of Estimated R_0 Values from the Initial DP ECM and the Complete ECM versus V_{OCV}

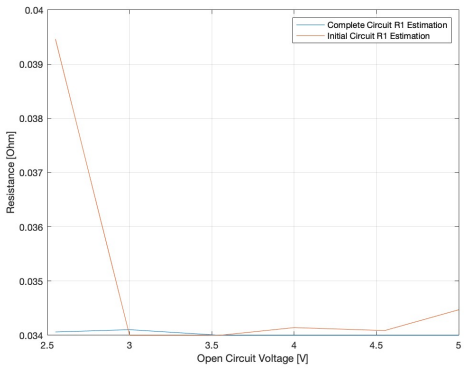

Figure 46: Graph with Comparison of Estimated R_1 Values from the Initial DP ECM and the Complete ECM versus V_{OCV}

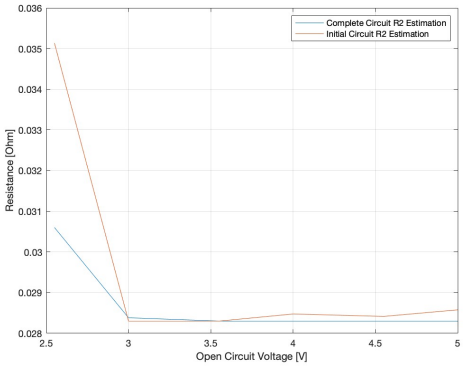

Figure 47: Graph with Comparison of Estimated R_2 Values from the Initial DP ECM and the Complete ECM versus V_{OCV}

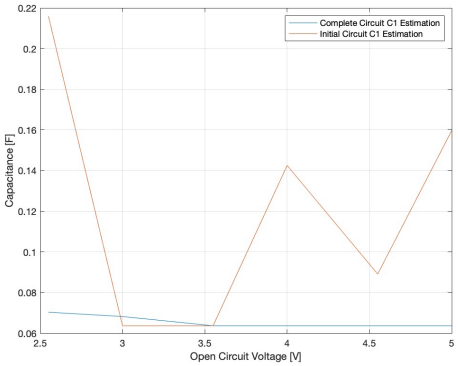

Figure 48: Graph with Comparison of Estimated C_1 Values from the Initial DP ECM and the Complete ECM versus V_{OCV}

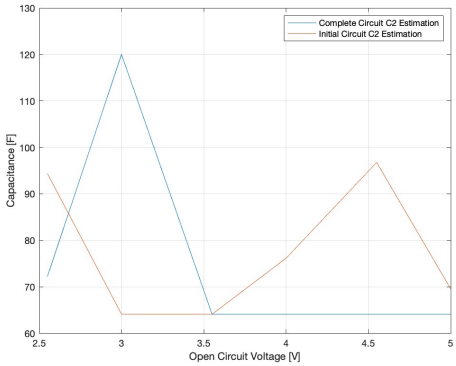

Figure 49: Graph with Comparison of Estimated C_2 Values from the Initial DP ECM and the Complete ECM versus V_{OCV}

The calculated error for each parameter R_0, R_1, R_2, C_1, and C_2 are illustrated in Figure 50, Figure 51, Figure 52, Figure 53, and Figure 54 respectively.

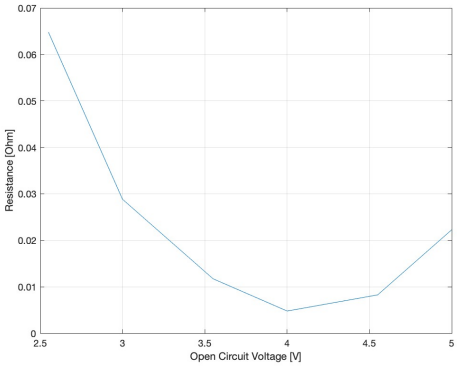

Figure 50: Graph with Calculated Error of R_0 Values from the Initial DP ECM and the Complete ECM versus V_{OCV}

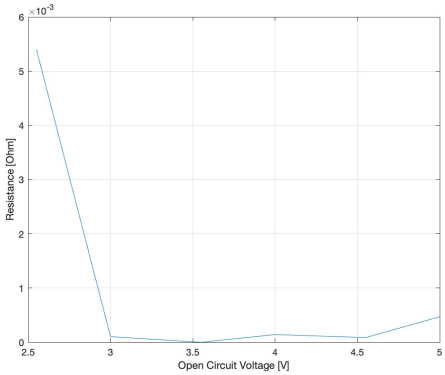

Figure 51: Graph with Calculated Error of R_1 Values from the Initial DP ECM and the Complete ECM versus V_{OCV}

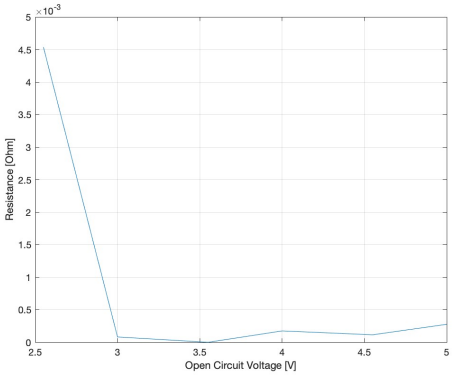

Figure 52: Graph with Calculated Error of R_2 Values from the Initial DP ECM and the Complete ECM versus V_{OCV}

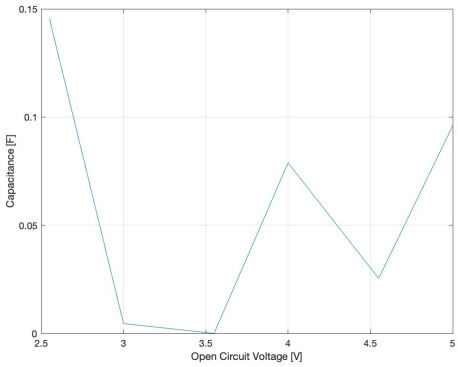

Figure 53: Graph with Calculated Error of C_1 Values from the Initial DP ECM and the Complete ECM versus V_{OCV}

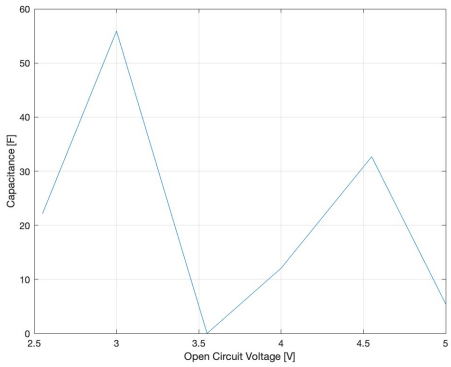

Figure 54: Graph with Calculated Error of C_2 Values from the Initial DP ECM and the Complete ECM versus V_{OCV}

5 Discussion

5.1 Initial Dual Polarisation Model Discussion

The estimated parameter values, R_0, R_1, R_2, C_1, and C_2 taken from the initial values given in [29] show some variation. The initial values from [29], shown in Table 1, somewhat correspond to the estimated parameters found using the MATLAB Optimization script. Looking at the derived estimated parameter values, found in Table 2, for the same initial V_{OCV} value, the derived parameter values for R_0, R_1, and R_2 do not differ. On the other hand, looking at parameter values C_1 and C_2, the values differ greatly. Both C_1 and C_2 are a tenth of the value of the initial parameter values given in Table 1. This large difference could be due to a few factors. One factor that could cause this is the method in which the parameters were estimated using data fitting models. In [29], the MATLAB *fminsearch* function was used, which differs from the MATLAB Optimization Toolbox that was used in this paper. This could lead to the difference in the estimated parameter values. Another factor that could influence this difference in capacitance values is the current input used in the HPPC test. In [29], the current input is a combination of positive and negative pulses with irregular timings. This could affect the time constants of the circuit. In this paper, a more regular current input is used with one positive and negative pulse. This could help the time constants of the circuit be more consistent and therefore the values of the capacitance are different.
Regarding the results from the initial Dual Polarisation model, there is a slight variation between the simulated voltage response and the estimated parameter voltage response, in the order of 10^{-6} difference for the different input voltages. The only voltage response error greater than 10^{-6} is for the input voltage of 1.55V. This is due to a few different factors. Initially, this very slight difference is due to the final parameter values derived from the MATLAB Optimization script. One way to fix this small difference would be to improve the optimization script by defining better boundaries. By defining better boundaries, the MATLAB Optimization can cycle through more possible parameter value combinations to find the values with the most Pareto efficiency for each parameter. Another way to fix the small difference in values could be by increasing the sample time of the MATLAB simulation. Increasing the sample time allows for more data points to be used in the derivation of the parameter values, allowing for a better and more accurate result.

5.2 Complete Circuit Model Discussion

Due to simulating an array of batteries instead of a single battery, as done for the initial parameter estimations, some assumptions need to be made. To ensure that the chosen battery could be used, an array of ten batteries in series is assumed. Furthermore, it is assumed that all ten batteries have the same internal component values. This meant multiplying the resistance values by ten and dividing the capacitance values by ten to ensure that they correspond to the ten batteries in series. Due to this, the values used for the OCV are also multiplied by ten to fit the new model parameters. This does add a lot of uncertainty to the model as all these assumptions need to be incorporated.
From the parameter estimation, it can be seen that the parameters do follow the initial estimated parameters seen in Table 2. There are some outliers in the complete circuit estimated values, as seen in Table 3. This is also illustrated better in Figure 45, Figure 46, Figure 47, Figure 48, Figure 49. This can be due to a few factors. Initially, this could be due to the data fitting model script and the boundaries set within the DFM. By setting the lower boundary values at a tenth of the maximum boundary values, a limited range is used. This could limit the values that the MATLAB Optimization script uses, and therefore the most accurate value is not found. Additionally, due to the HPPC signal used, the estimated parameters could be skewed as the HPPC signal does have some errors, as illustrated in Figure 42 and Figure 43. This could lead to errors within the DFM, as it uses the generated signal from the complete circuit DP ECM HPPC signal as an input in the parameter estimation script. Furthermore, errors within the code used to graph the estimated values could also contain errors, causing discrepancies in the data. The data

results show that the chosen data fitting model does work fairly well but further optimisation is required. To overcome any further issues, improvements could be made to the DFM to limit errors in further testing. Additionally, accuracy of simulations vary with the step-size used in Simulink. Therefore using a lower step-size could also improve the accuracy of the data used in the DFM.
The parameters were obtained by only simulating the converter circuit and the battery model. The H-Bridge controller was not designed in time and therefore could not be used. This is illustrated in Figure 44, as the plotted signal increases in amplitude during the simulation. For further development, the controller for the H-Bridge needs to be refined to ensure that the complete circuit works. Additionally, improving the filter used to link the H-Bridge and the Bi-Directional converter could ensure that there is less ripple in the output.
Looking at the voltage response graphs, there are some errors between the calculated and the simulated values. This can be due to a few factors. Initially, this could be due to the noise within the system. By not reducing the noise further, the DFM has a much larger input range. This could lead to errors in the parameter estimation, which when compounded with the calculations that use the same signals, causes the errors in the voltage response. From the calculated error, it can be seen that the voltage error is quite large in some cases. This is particularly evident in Figure 81-Figure 82 and in Figure 83-Figure 84, where the difference between the estimated voltage response in red and the simulated voltage response in black vary during the peak of the HPPC input. Apart from the estimated parameter values, this could also be due to the simulation settings. Due to MATLAB's limitation of data that can be used in the DFM, the range of data is very limited. This made it very difficult to reduce the noise as the stepping size of the simulation could not be decreased to improve the accuracy of the simulation. For future simulations, a larger data set and a lower stepping size could help reduce the noise of the circuit and therefore improve not only the calculated voltage response but also the estimated parameters.
Regarding the State of Charge, it can be seen that due to the HPPC current, the SoC does change. This is evident in Figure 39 - Figure 41. Due to the HPPC, the measured voltage across the battery before and after the test does vary. This indicates the State of Charge of the battery varies with the HPPC input signal. Again, similar to the results of the voltage response, this could be due to the simulation of the model. By having to limit the time the simulation can run but ensuring that the HPPC is as accurate as possible, as discussed in subsection 3.4, the model is not able to fully settle after the second pulse. To ensure that this doesn't happen in future simulations, a longer simulation time could be beneficial. Furthermore, reducing noise could also improve the SoC, as the large value range increases the cumulative error.
Regarding the HPPC signals from the converter, it can be seen that they are not completely square. This, similar to the issues outlined already, is due to the combination of the stepping size and the simulation run time. Allowing the simulation to run for longer with a smaller stepping size would increase the accuracy of the HPPC currents. Furthermore, fine-tuning the inductor value and the PI controller value could also improve the measured HPPC signal from the converter circuit. Improving these factors could reduce the error in the HPPC signal, which would improve many of the errors encountered in the simulations and results.

5.3 Comparison Between Initial and Complete Circuit Models

Looking at the comparison of the initial model and the complete model, it can be seen that there are some differences. As outlined above, an assumption of ten batteries in series is made. This does change the values, but as can be seen from the results, the values are closely correlated. This is better illustrated in Figure 45 - Figure 54. There are a few values for C1 and C2 that are quite different, but this could be due to the simulation time, the data fitting model, and the noise within the system, as mentioned previously. Furthermore, there are large errors present in parameter values between the initial DP ECM and the complete DP ECM at lower OCV values. This, similar to what has already been mentioned could be due to many factors within the DFM and the simulation, which carry over and become compounded as the simulated signals are used for further calculations.
Secondly, looking at the voltage response of the two models, it can be seen that the maximum

values attained during the simulation do vary slightly. This, again could be due to the parameter values and the assumption of ten batteries in series. Furthermore, due to using a perfect HPPC signal in the initial model, and the HPPC signal in the complete model, there are some errors that could be introduced, when calculating the voltage error, compound the total error of the system. Using a more perfect HPPC signal could improve the results of the voltage response. This, as outlined above, can be done by improving the PI controller values and the inductor value within the converter circuit.
Lastly, due to a lack of time, SoH estimations could not be done. To do this within this model, a method to degrade the battery values is needed. For future improvements, this would need to be taken into consideration.

6 Conclusion

Through the simulations done in this paper, it can be seen that the principle of using a converter circuit as an HPPC signal generator for battery parameter estimation does work. Furthermore, the integration of an H-Bridge is also feasible. Having an H-Bridge, which can be connected to power the converter for different battery voltages and sizes of battery arrays, allows for a wider range of batteries to tested. From the outcomes of this paper, it can be seen that further improvements in the simulations can lead to a more accurate SoH method. This includes improvements in controlling the H-Bridge and the Bi-Directional converter, improving the simulation settings regarding step-size and data size, and reducing noise within the simulation. Doing these steps could lead to further developments and actual construction of the complete circuit.

7 Appendix

7.1 AI Statement

Artificial Intelligence (AI) was used in this paper. Spellcheck and autocorrect from Grammerly and Overleaf were used as a means to ensure that the grammar and the spelling were consistent, and that no simple writing mistakes are found in the text. After use of these tools, I have reviewed and edited the content as needed. I take full responsibility of the content of this work.

7.2 Initial Estimated Parameter Values

Table 2: Initial Estimated Parameter Values

Parameter	**Parameter Values**											
$V_{OCV}[V]$	0	0.55	1	1.55	2	2.55	3	3.55	4	4.55	5	5.55
$R_0[\Omega]$	0.1628	0.1800	0.2282	0.1421	0.1641	0.0830	0.1494	0.0473	0.0905	0.0784	0.1222	0.0965
$R_1[\Omega]$	0.0360	0.0384	0.0368	0.0361	0.0342	0.0394	0.0340	0.0340	0.0341	0.0340	0.0344	0.0343
$R_2[\Omega]$	0.0341	0.0291	0.0296	0.0287	0.0296	0.0351	0.0283	0.0283	0.0284	0.0284	0.0285	0.0303
$C_1[F]$	0.1969	0.1622	0.3342	0.0778	0.2017	0.2159	0.0637	0.0637	0.1425	0.0891	0.1597	0.2316
$C_2[F]$	215.79	155.40	81.789	73.089	75.708	94.354	64.100	64.100	76.164	96.762	69.530	119.46

7.3 Voltage Response of Initial Dual Polarisation Model

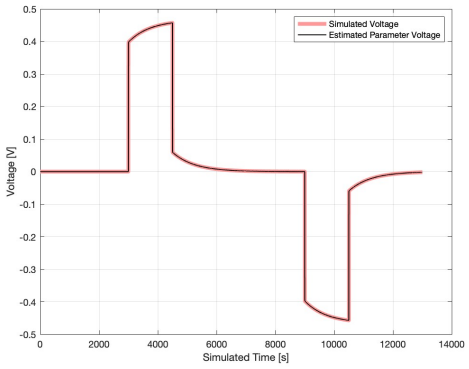

Figure 55: Voltage Response of Dual Polarisation Equivalent Circuit Model for Input Voltage of 0V

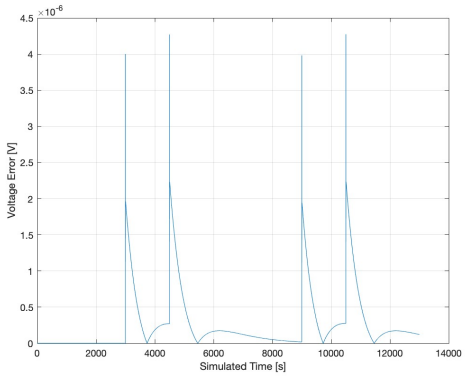

Figure 56: Voltage Response Error of Simulated Voltage and Calculated Voltage for Input Voltage of 0V

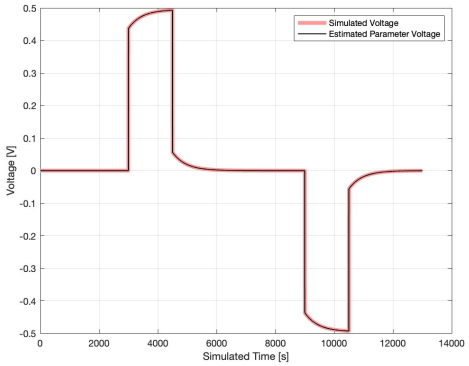

Figure 57: Voltage Response of Dual Polarisation Equivalent Circuit Model for Input voltage of 0.55V

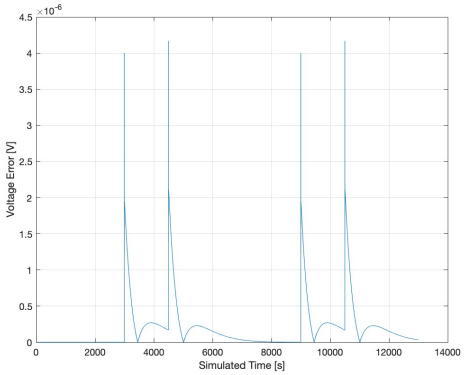

Figure 58: Voltage Response Error of Simulated Voltage and Calculated Voltage for Input Voltage of 0.55V

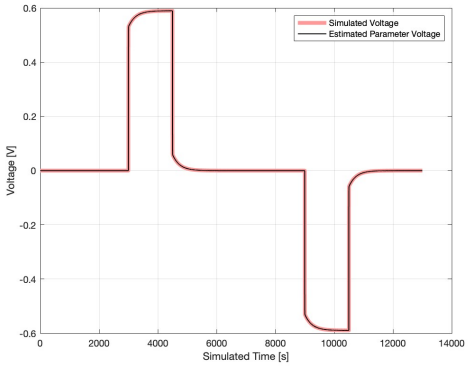

Figure 59: Voltage Response of Dual Polarisation Equivalent Circuit Model for Input voltage of 1V

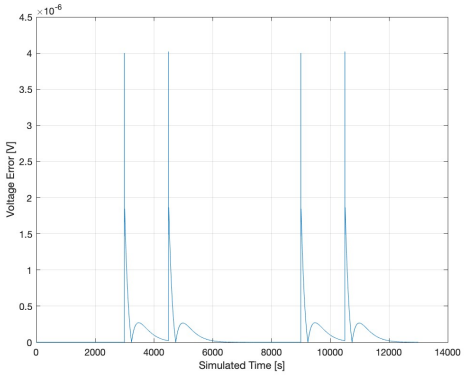

Figure 60: Voltage Response Error of Simulated Voltage and Calculated Voltage for Input Voltage of 1V

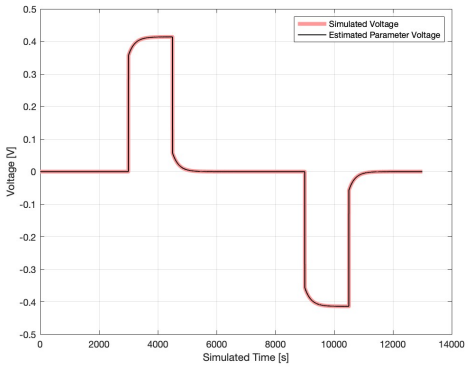

Figure 61: Voltage Response of Dual Polarisation Equivalent Circuit Model for Input voltage of 1.55V

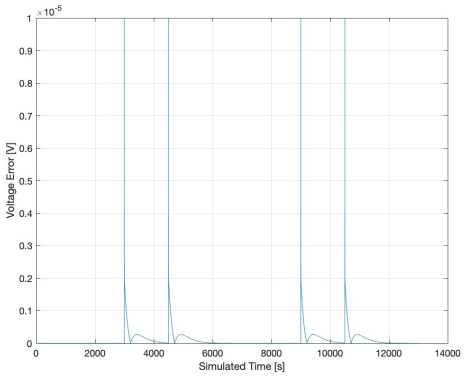

Figure 62: Voltage Response Error of Simulated Voltage and Calculated Voltage for Input Voltage of 1.55V

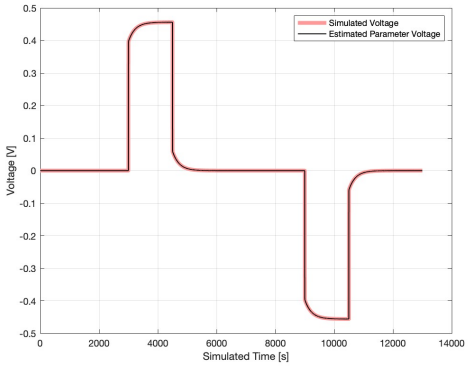

Figure 63: Voltage Response of Dual Polarisation Equivalent Circuit Model for Input voltage of 2V

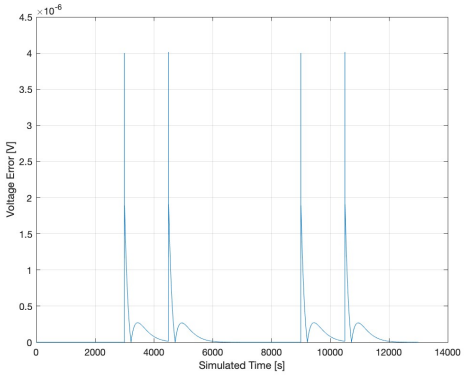

Figure 64: Voltage Response Error of Simulated Voltage and Calculated Voltage for Input Voltage of 2V

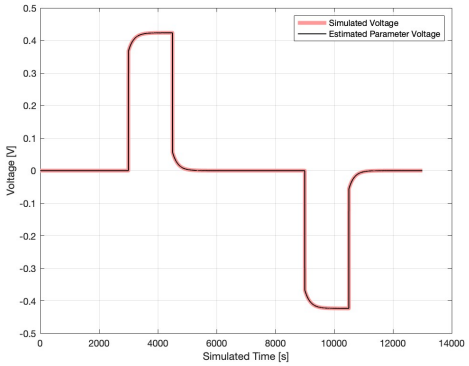

Figure 65: Voltage Response of Dual Polarisation Equivalent Circuit Model for Input voltage of 3V

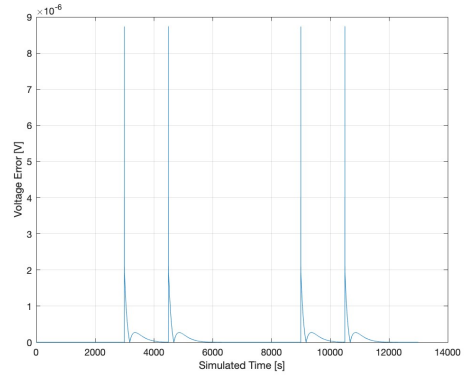

Figure 66: Voltage Response Error of Simulated Voltage and Calculated Voltage for Input Voltage of 3V

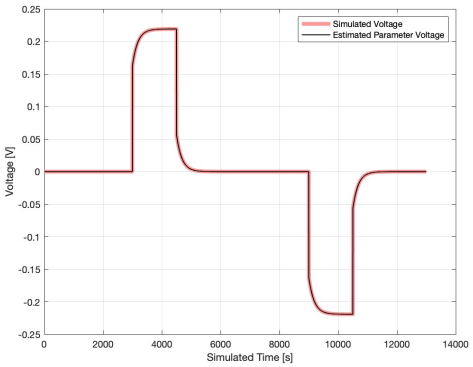

Figure 67: Voltage Response of Dual Polarisation Equivalent Circuit Model for Input voltage of 3.55V

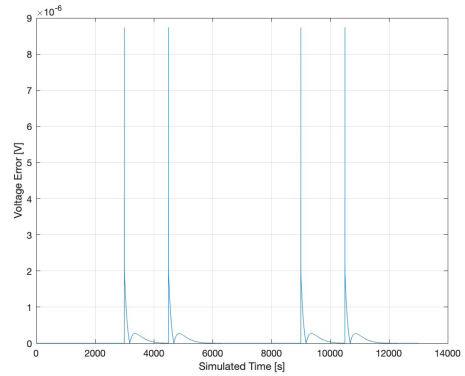

Figure 68: Voltage Response Error of Simulated Voltage and Calculated Voltage for Input Voltage of 3.55V

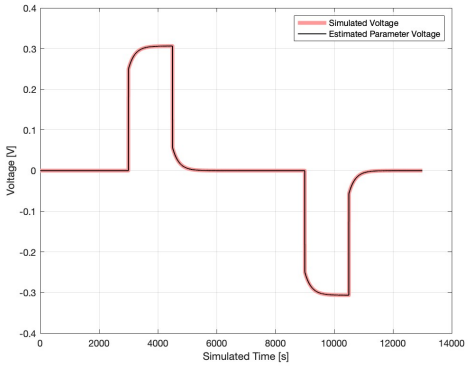

Figure 69: Voltage Response of Dual Polarisation Equivalent Circuit Model for Input voltage of 4V

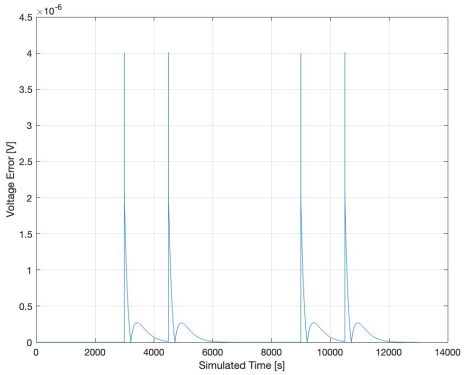

Figure 70: Voltage Response Error of Simulated Voltage and Calculated Voltage for Input Voltage of 4V

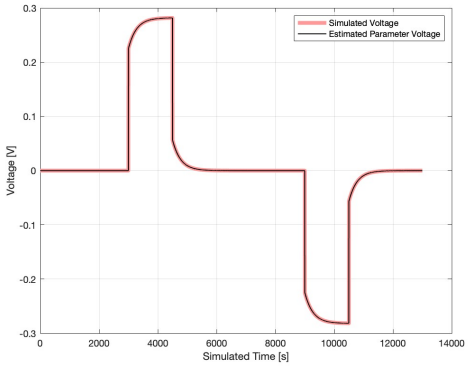

Figure 71: Voltage Response of Dual Polarisation Equivalent Circuit Model for Input voltage of 4.55V

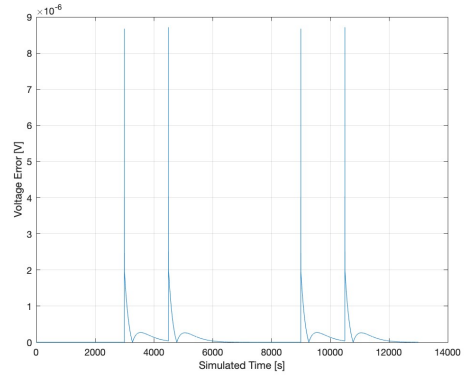

Figure 72: Voltage Response Error of Simulated Voltage and Calculated Voltage for Input Voltage of 4.55V

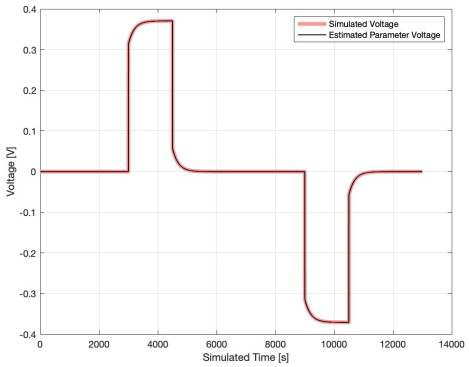

Figure 73: Voltage Response of Dual Polarisation Equivalent Circuit Model for Input voltage of 5V

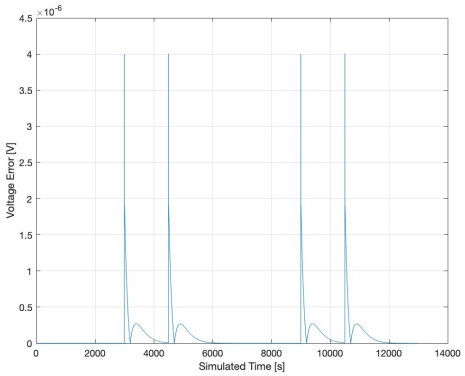

Figure 74: Voltage Response Error of Simulated Voltage and Calculated Voltage for Input Voltage of 5V

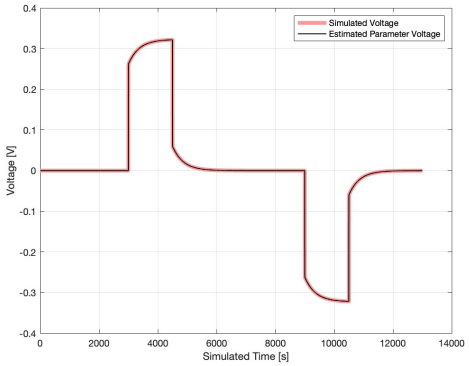

Figure 75: Voltage Response of Dual Polarisation Equivalent Circuit Model for Input voltage of 5.55V

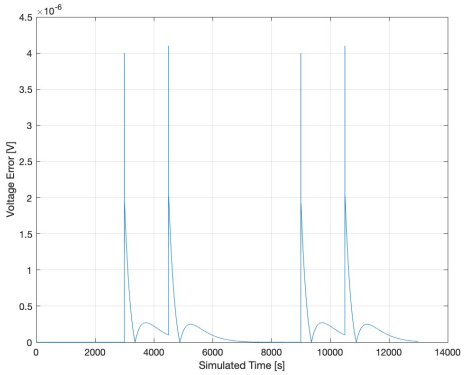

Figure 76: Voltage Response Error of Simulated Voltage and Calculated Voltage for Input Voltage of 5.55V

7.4 Complete Circuit Estimated Parameter Values

Table 3: Complete Circuit Estimated Parameter Values

Parameter	**Parameter Values**					
V_{OCV} [V]	25.5	30	35.5	40	45.5	50
$R_0[\Omega]$	0.0182	0.1206	0.0590	0.0953	0.0701	0.100
$R_1[\Omega]$	0.03406	0.0341	0.0340	0.0340	0.0340	0.0340
$R_2[\Omega]$	0.0306	0.02838	0.0283	0.0283	0.0283	0.0283
$C_1[F]$	0.0703	0.0682	0.0637	0.0637	0.0637	0.0637
$C_2[F]$	72.235	120.00	64.100	64.100	64.100	64.100

7.4.1 Voltage Response of Complete Dual Polarisation Model

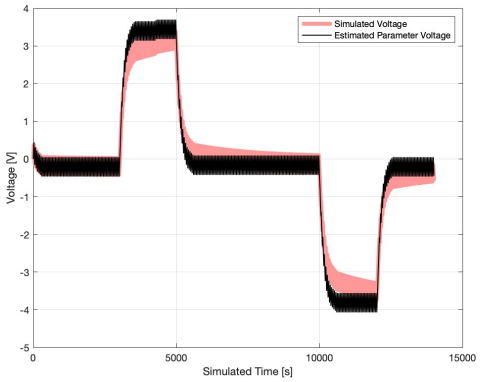

Figure 77: Voltage Response of Complete Circuit with Initial V_{OCV} Value of 30V

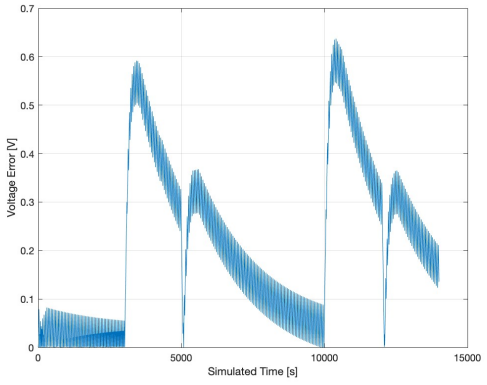

Figure 78: Voltage Response Error of Simulated Voltage and Calculated Voltage for Input V_{OCV} of 30V

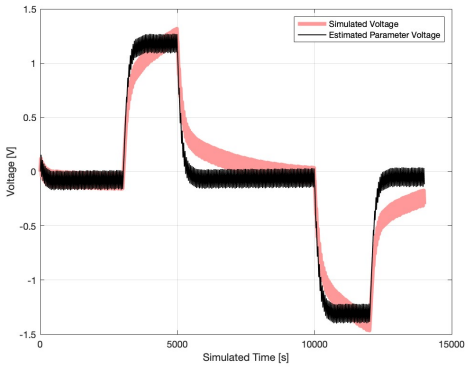

Figure 79: Voltage Response of Complete Circuit with Initial V_{OCV} Value of 35.5V

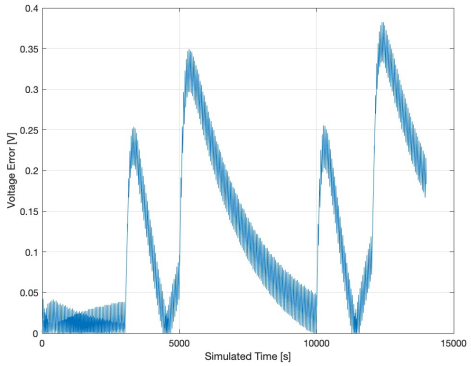

Figure 80: Voltage Response Error of Simulated Voltage and Calculated Voltage for Input V_{OCV} of 35.5V

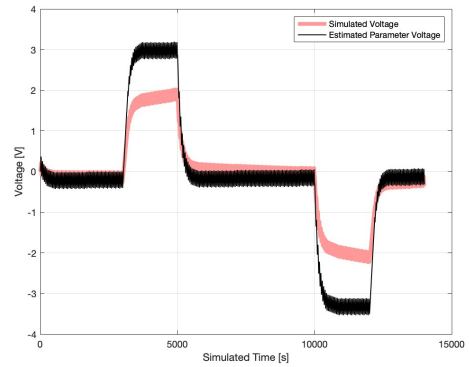

Figure 81: Voltage Response of Complete Circuit with Initial V_{OCV} Value of 40V

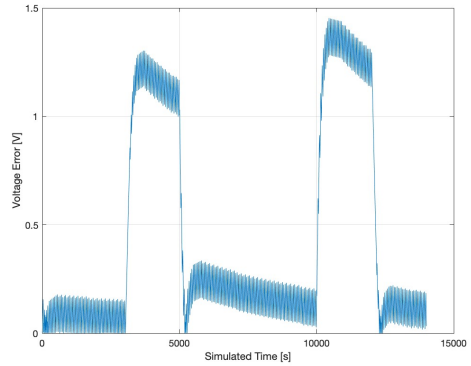

Figure 82: Voltage Response Error of Simulated Voltage and Calculated Voltage for Input V_{OCV} of 40V

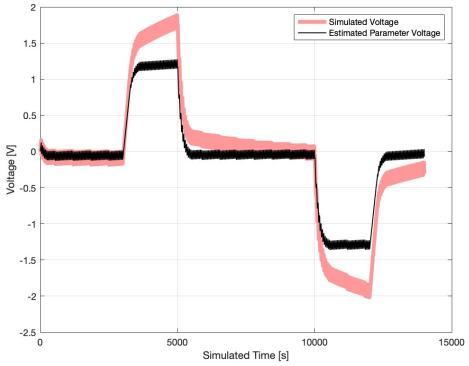

Figure 83: Voltage Response of Complete Circuit with Initial V_{OCV} Value of 45.5V

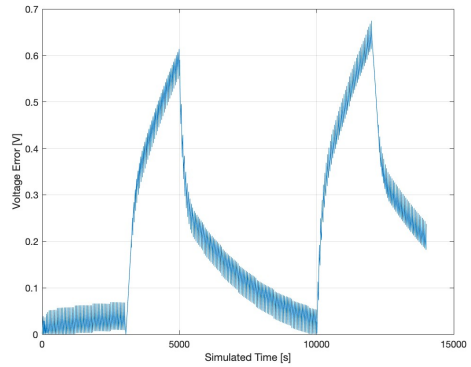

Figure 84: Voltage Response Error of Simulated Voltage and Calculated Voltage for Input V_{OCV} of 45.5V

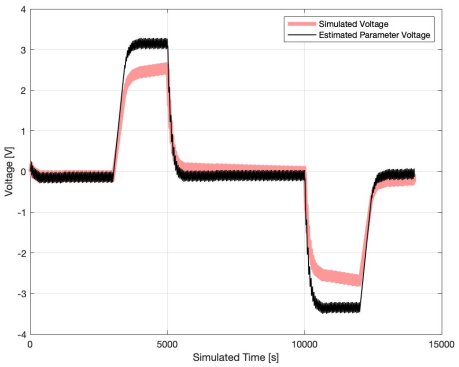

Figure 85: Voltage Response of Complete Circuit with Initial V_{OCV} Value of 50V

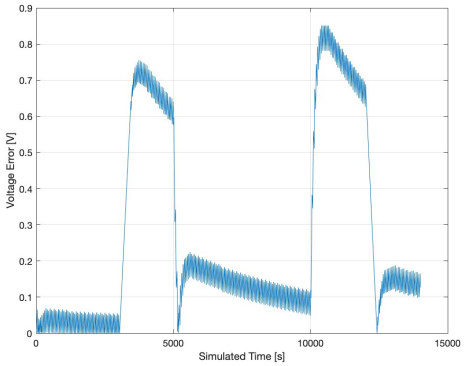

Figure 86: Voltage Response Error of Simulated Voltage and Calculated Voltage for Input V_{OCV} of 50V

References

[1] C. G. Colombo, M. Longo, and D. Zaninelli, *Batteries: Advantages and Importance in the Energy Transition.* Cham: Springer International Publishing, 2024, pp. 69–82. [Online]. Available: https://doi.org/10.1007/978-3-031-48359-2_5

[2] M. Alimawi, "Cascaded h-bridge converter integrated with split batteries and with multilevel ac output for household applications," 2023.

[3] A. Barai, K. Uddin, W. Widanage, A. McGodrdan, and P. Jennings, "A study of the influence of measurement timescale on internal resistance characterisation methodologies for lithium-ion cells," *Scientific Reports 8*, 2018.

[4] R. Xiong, L. Li, and J. Tian, "Towards a smarter battery management system: A critical review on battery state of health monitoring methods," *Journal of Power Sources*, vol. 405, pp. 18–29, 2018. [Online]. Available: https://www.sciencedirect.com/science/article/pii/S037877531831111X

[5] P. Venugopal and T. Vigneswaran, "State-of-health estimation of li-ion batteries in electric vehicle using indrnn under variable load condition," *Energies*, 2019. [Online]. Available: https://www.mdpi.com/1996-1073/12/22/4338

[6] M. Inc. [Online]. Available: https://nl.mathworks.com/products/simulink.html

[7] Y. Fu, J. Xu, M. Shi, and X. Mei, "A fast impedance calculation-based battery state-of-health estimation method," *IEEE Transactions on Industrial Electronics*, 2022. [Online]. Available: https://ieeexplore.ieee.org/document/9492805

[8] M. Prine-Robie, "How does temperature affect battery performance?" [Online]. Available: https://www.greentechrenewables.com/article/how-does-temperature-affect-battery-performance

[9] D. Ouyang, J. Weng, M. Chen, and J. Wang, "Impact of high-temperature environment on the optimal cycle rate of lithium-ion battery," *Journal of Energy Storage*, vol. 28, p. 101242, 2020. [Online]. Available: https://www.sciencedirect.com/science/article/pii/S2352152X19315506

[10] D. Linden, *Handbook of Batteries.* McGraw-Hill, 2001, ch. 3: Factors Affecting Battery Performance.

[11] J. Sun and J. Kainz, "Optimization of hybrid pulse power characterization profile for equivalent circuit model parameter identification of li-ion battery based on taguchi method," *Journal of Energy Storage*, vol. 70, p. 108034, 2023. [Online]. Available: https://www.sciencedirect.com/science/article/pii/S2352152X23014317

[12] T. Białoń, R. Niestrój, W. Skarka, and W. Korski, "Hppc test methodology using lfp battery cell identification tests as an example," *Energies*, 2023. [Online]. Available: https://www.mdpi.com/1996-1073/16/17/6239

[13] Y. Zheng, Z. Shi, D. Guo, H. Dai, and X. Han, "A simplification of the time-domain equivalent circuit model for lithium-ion batteries based on low-frequency electrochemical impedance spectra," *Journal of Power Sources*, vol. 489, p. 229505, 2021. [Online]. Available: https://www.sciencedirect.com/science/article/pii/S0378775321000549

[14] S. N. David, "Pulse power characterisation for lithium ion cells in automotive applications," 2016. [Online]. Available: https://publications.lib.chalmers.se/records/fulltext/241112/241112.pdf

[15] I. Jarrraya, L. Degaa, N. Rizoug, M. H. Chabchoub, and H. Trabelsi, "Comparison study between hybrid nelder-mead particle swarm optimization and open circuit voltage—recursive least square for the battery parameters estimation," *Journal of Energy Storage*, 2022.

[16] T. Soeiro and H. de Vries, "Simple and low cost portable battery tester for equivalent circuit model determination implementing the hybrid pulsed power cycling method," this is not a published paper, but was sent to me by my supervisor Thiago Batista Soeiro.

[17] J. Peng, J. Meng, J. Wu, Z. Deng, M. Lin, S. Mao, and D.-I. Stroe, "A comprehensive overview and comparison of parameter benchmark methods for lithium-ion battery application," *Journal of Energy Storage*, vol. 71, p. 108197, 2023. [Online]. Available: https://www.sciencedirect.com/science/article/pii/S2352152X23015943

[18] M. Zhang, S. Wang, X. Yang, W. Xu, X. Yang, and C. Fernandez, "A novel square root adaptive unscented kalman filter combined with variable forgetting factor recursive least square method for accurate state-of-charge estimation of lithium-ion batteries," *International Journal of Electrochemical Science*, vol. 17, no. 9, p. 220915, 2022. [Online]. Available: https://www.sciencedirect.com/science/article/pii/S145239812301101X

[19] D. Liu, S. Wang, Y. Fan, Y. Liang, C. Fernandez, and D.-I. Stroe, "State of energy estimation for lithium-ion batteries using adaptive fuzzy control and forgetting factor recursive least squares combined with aekf considering temperature," *Journal of Energy Storage*, vol. 70, p. 108040, 2023. [Online]. Available: https://www.sciencedirect.com/science/article/pii/S2352152X23014378

[20] Y. Xie, S. Wang, G. Zhang, Y. Fan, C. Fernandez, and J. M. Guerrero, "Improved lumped electrical characteristic modeling and adaptive forgetting factor recursive least squares-linearized particle swarm optimization full-parameter identification strategy for lithium-ion batteries considering the hysteresis component effect," *Journal of Energy Storage*, 2023.

[21] T. Kalogiannis, M. S. Hosen, M. A. Sokkeh, S. Goutam, J. Jaguemont, L. Jin, G. Qiao, M. Berecibar, and J. Van Mierlo, "Comparative study on parameter identification methods for dual-polarization lithium-ion equivalent circuit model," *Energies*, 2019.

[22] A. M. Alsabari, M. K. Hassan, A. Che Soh, and R. Zafira, "Modeling and validation of lithium-ion battery with initial state of charge estimation," *Indonesian Journal of Electrical Engineering and Computer Science*, 2021.

[23] M. Gosso, R. Rolli, I. Ahmed, D. Jöst, W. Li, O. Rahbi, M. Soltani, R. Sonnenberger, and M. Montaru, "Technical specifications and test protocols for the battery," 3beLiEVe, Tech. Rep., 2020. [Online]. Available: https://www.3believe.eu/wp-content/uploads/2021/03/D1.2-Technical-specifications-and-test-protocols-for-the-battery.pdf

[24] C. Love and D. Hayman, "Battery test manual for baselining 'i&' benchmarking pre-commercial cells," US Naval Research Laboratory, Tech. Rep., 2022. [Online]. Available: https://apps.dtic.mil/sti/pdfs/AD1182429.pdf

[25] BatterijService, "Sanyo ncr18650ga unprotected 3500mah." [Online]. Available: https://www.batterijservice.nl/en/sanyo-ncr18650ga-3500mah-unprotected.html

[26] W. Li, L. Liang, W. Liu, and X. Wu, "State of charge estimation of lithium-ion batteries using a discrete-time nonlinear observer," *IEEE Transactions on Industrial Electronics*, 2017.

[27] MATLAB, "gamultiobj." [Online]. Available: https://nl.mathworks.com/help/gads/gamultiobj.html

[28] M. Alimawi, R. Eskandari, P. Venugopal, and T. B. Soeiro, "Cascaded h-bridge converter integrated with split batteries and with multilevel ac output for household applications," *IEEE Applied Power Electronics Conference and Exposition*, 2024.

[29] H. de Vries and M. Appelman, "Portable state of power determination of li-ion battery cells," 2023. [Online]. Available: http://essay.utwente.nl/94725/1/deVries_MA_EEMCS.pdf

[30] El-Pro-Cus, "What is a full wave rectifier : Circuit with working theory." [Online]. Available: https://www.elprocus.com/full-wave-rectifier-circuit-working-theory/

[31] E. Tutorials, "Full wave rectifier." [Online]. Available: https://www.electronics-tutorials.ws/diode/diode_6.html

[32] B. Subedi, "Full wave rectifier basics, circuit, working 'i&' applications." [Online]. Available: https://how2electronics.com/full-wave-rectifier-basics-circuit-working-applications/

[33] J. Pala, "Full-wave rectifier." [Online]. Available: https://ecstudiosystems.com/discover/textbooks/basic-electronics/rectifiers/full-wave-rectifier/

[34] El-Pro-Cus, "What is pi filter : Circuit, working and its applications." [Online]. Available: https://www.elprocus.com/pi-filter-circuit-working-and-its-applications/

[35] InstrumentationTools, "pi filter operation." [Online]. Available: https://instrumentationtools.com/pi-filter-operation/

[36] DaeNotes, "Filter circuits." [Online]. Available: https://www.daenotes.com/electronics/devices-circuits/filter-circuits

[37] CadencePCBSolutions, "Passive pi filter design and simulation." [Online]. Available: https://resources.pcb.cadence.com/blog/2020-passive-pi-filter-design-and-simulation

[38] R. Darbali-Zamora, J. E. Quiroz, J. Hernandez-Alvidrez, J. Johnson, and E. I. Ortiz-Rivera, "Viability assessment of a real-time simulation model for a residential dc microgrid network to compensate electricity disturbances in puerto rico," *2018 IEEE Andescon*, 2018.

[39] B. Li, C. Xu, C. Li, and Z. Guan, "Working principle analysis and control algorithm for bidirectional dc/dc converter," *Journal of Power Technologies*, vol. 97, pp. 327–335, 09 2017.

[40] S. B. Prakash and G. Singh, "Bidirectional buck-boost converter in solar pv system for supercapacitor energy storage system," in *Smart and Intelligent Systems*, S. Dawn, K. N. Das, R. Mallipeddi, and D. P. Acharjya, Eds. Singapore: Springer Singapore, 2022, pp. 145–156.

[41] A. Wallberg, "Design and construction of a bidirectional dc/dc converter," Master's thesis, Uppsala Universitet, 2019. [Online]. Available: https://www.diva-portal.org/smash/get/diva2:1323585/FULLTEXT01.pdf

[42] S. H. Khan, A. M. A. Khan, and A. Saleque, "H-bridge driven propulsion system for a light weight electric vehicle using dc link voltage controller," 12 2017.

[43] K. Tytelmaier, O. Husev, O. Veligorskyi, and R. Yershov, "A review of non-isolated bidirectional dc-dc converters for energy storage systems," 10 2016, pp. 22–28.

[44] GatesEnergyProducts, "Section 4 - sealed lead cells and batteries," in *Rechargeable Batteries Applications Handbook*, ser. EDN Series for Design Engineers. Newton: Newnes, 1998, pp. 153–235. [Online]. Available: https://www.sciencedirect.com/science/article/pii/B978075067006750005X